CEBAF PROPOSAL COVER SHEET

This Proposal must be mailed to:

CEBAF
Scientific Director's Office
12000 Jefferson Avenue
Newport News, VA 23606

and received on or before OCTOBER 30, 1989

A. TITLE: "Radiative Decays of the Low-Lying Hyperons"

B. CONTACT PERSON: G. S. Mutchler

ADDRESS, PHONE AND BITNET:

713-528-2159 MUTCH@RICE
Bonner Nuclear Laboratory-Rice University
Houston, TX 77251-1892

C. THIS PROPOSAL IS BASED ON A PREVIOUSLY SUBMITTED LETTER OF INTENT

☒ YES
☐ NO

IF YES, TITLE OF PREVIOUSLY SUBMITTED LETTER OF INTENT

Same as above

D. ATTACH A SEPARATE PAGE LISTING ALL COLLABORATION MEMBERS AND THEIR INSTITUTIONS

==========

(CEBAF USE ONLY)

Letter Received 10-31-89

Log Number Assigned PR-89-024

By KES
contact: Mutchler

RADIATIVE DECAYS OF THE LOW-LYING HYPERONS

D. L. Adams, B. E. Bonner, J. A. Buchanan, J. M. Clement,
M. D. Corcoran, H. E. Miettinen, G. S. Mutchler, and J. B. Roberts
T. W. Bonner Laboratories, Physics Department
RICE UNIVERSITY,
Houston, TX 77251-1892

M. Eckhause, A. Hancock, J. Kane, Y. Kuang, R. Welsh, and R. Winter
Department of Physics
COLLEGE of WILLIAM and MARY
Williamsburg, VA 23185

The CLAS Collaboration

ABSTRACT

We propose to measure the branching ratios of the electromagnetic decays of the low lying excited hyperons, using the CEBAF LAS. An excited hyperon will be produced using a tagged photon beam with $\Delta E_\gamma/E_\gamma = 0.25\%\ FWHM$, via the reaction $\gamma p \rightarrow K^+ Y^{*}$. The kaon, decay γ and the proton and π^- from the final state Λ will be detected. The four momentum of the hyperon will be reconstructed from the beam photon energy and the kaon momentum. The four momentum of the Λ will be reconstructed from the proton and π^- momenta. FASTMC modeling of the system indicates that the hyperon mass will be determined to better than 5 Mev FWHM and the Λ mass to better than 2 $Mev\ FWHM$. With such good mass resolution the backgrounds due to π^0 decays can be efficiently suppressed for the $Y^{*} \rightarrow \gamma\Lambda$ decays. However, a large coverage, fine grained shower counter is required to reduce the π^0 background for $Y^{*} \rightarrow \gamma\Sigma^0$ decays.

I. Introduction

We propose to measure the electromagnetic branching ratios of the low lying states of the Λ and Σ hyperons. The accessible states and allowed electromagnetic decay modes are shown in Figure 1. Recent experimental activity[1-4] in this field has stimulated theoretical interest[5-10] in the electromagnetic decays. Much of this work is summarized in a paper by Goldman *et al.*[1] which is included as an Appendix. To summarize the points made in this paper, the ground states of the Λ and Σ^0 hyperons, in a simple three quark model, have ground states composed of an up, down and strange quark, all in an $S_{\frac{1}{2}}$ orbit. The light quarks are coupled to total spin and isospin $S = 0$ and $T = 0$ for the Λ and to $S = 1$ and $T = 1$ for the Σ^0 as shown in Figure 1. The strange quark is then coupled to give a $J = \frac{1}{2}^+$ ground state, with $T = 0$ for the Λ and $T = 1$ for the Σ^0. The excited states are formed by exciting one quark to a different spin or orbital state. Photoemission occurs by the deexcitation of this quark. The first $T = 1$ excited state is the $\Sigma^*(1385)$ with $J = \frac{3}{2}^+$. This is formed by a spin flip of the strange quark. This state can decay to either the $T = 0$ or the $T = 1$ ground state by an $M1$ transition. The first excited $T = 0$ state, the $\Lambda^*(1405)$, has a strange quark excited to the $P_{\frac{1}{2}}$ orbital, yielding a $J = \frac{1}{2}^-$ state. This can decay to the $T = 0$ ground state by an $E1$ transition. However, in the naive model we are considering here, the transition to either $T = 1$ state is strictly forbidden, as it would require a two quark interaction. The second excited state, the $\Lambda^*(1520)$, is predicted to be a linear combination of states with either a strange quark or one of the light quarks in the $P_{\frac{3}{2}}$ orbital, all coupled to a $J = \frac{3}{2}^-$ state. As before the $\Lambda^*(1520)$ is forbidden to decay to the $\Sigma^*(1385)$, due to the one-body nature of the electromagnetic operator.

The structure of these states is not well understood. The nature of the $\Lambda(1405)$ has been in dispute for many years. Originally it was interpreted as an antikaon-nucleon bound state[11]. With the advent of nonrelativistic quark models (NRQM) it was interpreted as a more or less normal three quark state[12] although it stands out in quark models as one state whose energy is particularly hard to fit. For example, the Isgur-Karl NRQM calculation predicts the center of gravity of the $\Lambda(1520)$ and $\Lambda(1405)$, but does not correctly predict the mass splitting. More recently cloudy bag

model (CBM) calculations by Veit *et al.*[13] find that the $\Lambda(1405)$ is predominately an antikaon-nucleon bound state with some small admixture of three quark states. It is very difficult to decide which interpretation is correct from strong interaction data alone, since the $\Lambda(1405)$, which is below the $\bar{K}N$ threshold, is seen only in $\Sigma\pi$ production and through its effect on the low-energy $\bar{K}N$ S-wave.

The best test of the internal structure of these hyperon states is a measurement of their electromagnetic transitions since these experiments should be significantly easier to interpret. The radiative widths have been calculated by a number of groups, and their results are listed in Table I. Darewych *et al.*[5] (DHK) used the Isgur-Karl[14] quark model. Moniz, Soyeur and Kaxiras[6] used a fixed radius static cavity approximation to the MIT bag model. Finally Kaxiras[6] used the Isgur-Karl model with two different sets of basis states, labelled $SU(6)$ and uds. The values quoted for the last three calculations are taken from ref. 1. As can be seen from Table I the theoretical values can vary by as much as a factor of 60, with the forbidden transitions allowed in some models. Furthermore, other models are possible, such as an admixture of $q^4\bar{q}$ states,[15] that lead to larger rates. See ref. 1 for further details. Thus the measurement of electromagnetic transition rates provide a very sensitive test of the various quark models. For example, DHK point out that a large radiative width for the $\Lambda^*(1520)$ and $\Lambda^*(1405)$ to the Σ's would imply that color hyperfine forces are present in these systems.

II. Existing Measurements

There are only a limited number of measurements of neutral hyperon electromagnetic decays. The radiative width of the $\Sigma^0(1193)$ to $\gamma\Lambda(1116)$ decay has been measured by Dydak *et al.*[16] to be $11.5 \pm 2.6keV$. There are two measurements of the radiative width of the $\Lambda(1520)$ to $\gamma\Lambda(1116)$ decay, using the reaction $K^-p \rightarrow \gamma\Lambda$. Mast *et al.*,[17] using a bubble chamber, found 258 events, 15% of which were assumed to be $\gamma\Sigma^0$ events. The amount of this background depends on the unmeasured $\Lambda(1520) \rightarrow \gamma\Sigma^0$ branching ratio. They obtained a radiative width of $150 \pm 30keV$. Their measured angular distribution was consistent with an E1 transition. A recent, unpublished, CERN experiment,[3] using a large NaI detector, found a radiative width in serious disagreement with Mast

et al. Finally there exists a weak upper limit on the radiative decay of the $\Sigma^0(1385)$ from Colas *et al.*[18] They find an upper limit of about $2000keV$, which does not constrain any of the models.

The branching ratio for radiative capture $K^-p \rightarrow \gamma\Lambda$ has been measured by Humphreys and Ross,[19], Davies *et al.*,[20] Lowe *et al.*[4] and Whitehouse *et al.*[2] Whitehouse *et al.* also have measured the $K^-p \rightarrow \gamma\Sigma^0$ branching ratio. The results for these experiments are given in Table II, along with the current theoretical predictions. The most precise results are due to Whitehouse *et al.*, who measured the photon spectrum from K^- stopping in a liquid hydrogen target with a high-resolution (1.5% $FWHM$ at 300 MeV) $NaI(Tl)$ detector. Their data are shown in Figure 2. They have a total of 499 $\gamma\Lambda$ events and 850 $\gamma\Sigma^0$ above a substantial γ continuum. Their results are a factor of two below the theoretical predictions. There is considerable controversy among theorists concerning the degree to which the K^-p radiative capture creates the $\Lambda(1405)$ as an intermediate state, which leads to theoretical uncertainties in extracting the radiative width from these data.[7,8,9,10]

In the experiment proposed here, these difficulties will not exist. A clean, tagged sample of Y^* will be created through the reaction $\gamma p \rightarrow K^+Y^*$. The radiative decay of the excited hyperon can then be observed free of strong interaction effects in the formation channel. Unfortunately, photoproduction does not distinguish between the $I = 0$ $\Lambda(1405)$ and the $I = 1$ $\Sigma^0(1385)$. This will present difficulties. Nevertheless, comparison of our results with the results of the $K^-p \rightarrow \gamma\Lambda, \gamma\Sigma^0$ experiments will give the theorists valuable new data against which to test their various models.

III. Technical Details of Proposed Experiment

A. Introduction

A beam of tagged hyperons can be produced by detecting the kaon from the reaction

$$\gamma p \rightarrow K^+\Lambda^*(\Sigma^*) \qquad (1)$$

using the proposed LAS.[21] A tagged photon beam will be used to reduce the background due to Møller scattering of electrons and to establish the kinematics of the initial state.

The radiative decay of the excited hyperon is then signalled by the decay sequence.

$$\gamma p \rightarrow K^+ Y^{*-} \rightarrow K^+ \gamma \Lambda \rightarrow K^+ \gamma p \pi^- \tag{2}$$

A typical event is shown in Figure 3. The four momentum of the Λ is reconstructed from the measured $\pi^- p$ momenta, while the four momentum of the excited hyperon is reconstructed from the beam photon energy and the kaon momentum. From this information the decay photon four momentum can be calculated. Substantial background suppression can be obtained by verifying that a photon was detected in the shower counter at the appropriate element of phase space.

The Λ^* radiative decays proceeding via the Σ^0 have a more complicated signature;

$$\gamma p \rightarrow K^+ Y^{*-} \rightarrow K^+ \gamma \Sigma^0 \rightarrow K^+ \gamma \gamma \Lambda \rightarrow K^+ \gamma \gamma p \pi^- \tag{3}$$

This requires the reconstruction of the Y^* and Λ four momentum as before, but now the detection of the Σ^0 decay photon is necessary to determine the three momentum of the Σ^0. (The four momentum could of course be determined if the photon energy were well determined. But this will not be the case for the $70 MeV$ photon. Thus we assume the Σ^0 mass and calculate the three momentum.) Again detection of the Y^* decay photon greatly suppresses the background. In this case however, it is really a part of the zero constraint fit, because each low energy photon contributes only two angles, due to the poor energy resolution of the shower counter. This will be discussed in more detail in the section on modeling. The most serious background is the emission of a π^0 instead of a photon in the Y^* decay. With radiative branching ratios of 10^{-2} to 10^{-3}, good π^0 suppression is essential.

B. FASTMC Simulation of the Experiment

The experiment has been simulated using the program, FASTMC.[22] The assumed system parameters are given in Table III. All parameters not listed are as given in the CDR. Schumacher[23] has shown that the acceptance of the LAS for $\gamma p \rightarrow K\Lambda$ is maximized by bending positive particles toward the beamline and reducing the magnetic field to 20% of full strength, (due to low momentum of the π^-). Therefore we have made the appropriate changes in FASTMC and adopted this set of conditions to insure

the π^0 gammas misidentified as the Σ^0 decay gamma. Imposing a second γ coincidence requirement greatly reduces this background, but also reduces the $\gamma\Sigma^0$ peak, as is shown in Figure 6b. The mass resolution is adequate, but the rate is quite low due to the limited shower counter coverage.

Figures 7, 8, and 9 show the FASTMC results for the reactions

$$\gamma p \rightarrow K^+ Y^* \tag{8}$$

where Y^* is either the $\Sigma^0(1385)$ or the $\Lambda(1405)$. Here a tagged photon beam of 0.7 E_e to 0.9 E_e with $E_e = 2.4\ GeV$ was used. Again the figures represent 100 hour's running. Since the $\gamma\Lambda$ and $\gamma\Sigma^0$ branching ratios are an order of magnitude smaller then in the $\Lambda(1520)$ decays, and the π^0 branching ratios are four times larger (See Table IV), the π^0 related backgrounds are much larger relative to the $\gamma\Lambda$ and $\gamma\Sigma^0$ signals. The $\gamma\Lambda$ decays are still well separated from the π^0 continuum, as shown in Figure 8. However the $\gamma\Sigma^0$ signal is overwhelmed by the π^0 background as shown in Figure 9a. In Figure 9b we can see a clear $\gamma\Sigma^0$ signal above about a 20% background. But increased shower counter coverage is needed to improve the count rate.

Figure 10 shows the $\Lambda(1405)$ and $\Sigma^0(1385)$ mass spectrum for events that satisfies the γ mass cut in Figures 5a and 8a. The figure represents 500 hours of data. Clearly it will be difficult to separate the $\Sigma^0(1385) \rightarrow \gamma\Lambda$ decays from the $\Lambda(1405)$ decays due to their large widths and low count rates.

C. Count Rates and Background Estimations

We assume a tagged photon beam with an intensity of $10^7\gamma/sec$ and an energy range of $0.7 - 0.9E_e$ for $E_e = 2.4\ GeV$, ($E_\gamma = 1.7 - 2.2\ GeV$), and $0.6 - 0.8\ E_e$ for $E_e = 3.2\ GeV$, ($E_e = 1.9 - 2.6\ GeV$). The total photoproduction cross section for Λ's and Σ^0's is about $1\mu b$ in the energy range E_γ between 1 and 2 GeV. The total cross section for $\Lambda(1520)$ photoproduction cross section is also about $1\mu b$ at 2.25 GeV.[25,26] The $\Lambda(1405)$ and $\Sigma^0(1385)$ total cross sections were taken to be comparable, lacking any other information. Therefore, using a liquid hydrogen target of $1.0g/cm^2$, the $\gamma p \rightarrow K^+ Y^*$ reaction rate is estimated to be about 6 events/ sec for each hyperon. These rates must be reduced by the $\Lambda \rightarrow p\pi^-$ branching ratio, (0.64), the branching

ratios leading to Λ's in the final state (See Table IV), the decay probabilities of the kaon and π^-, and the LAS acceptance.

From the FASTMC simulations, we find that the acceptance is about 8% for $K^+ - p - \pi^-$ events and 3% for $K^+ - p - \pi^- - \gamma$ events. The decays of the kaon and π^- further reduce the rate by a factor of four. Table Va gives the count rate per 100 hours for the various reactions.

These low data rates could be increased by the following methods:

1). Move the target upstream by 50 - 100 cm. This will increase the acceptance for the forward going K^+. However it will reduce the shower counter solid angle, and reduce the $\gamma\Sigma^0$ count rate.

2). Increase the beam intensity to 2×10^7 or even 3×10^7. This will increase the tagger deadtime $2 - 3$ fold, and the accidental triggers due to the reaction $\gamma p \rightarrow \pi^+ p \pi^-$ $4 - 9$ fold. This may generate too many accidental events which could overload the Level 4 trigger and lead to too many events being written to tape. A possible solution to this problem might be to install a scintillating fiber vertex detector around the liquid hydrogen counter. A vertex detector with nanosecond response time would eliminate the accidentals from adjacent machine bunches and greatly reduce the trigger rate. The Rice University group will explore the design of such a detector.

3). Add a small, good energy resolution photon detector in the back angles ($60^0 - 160^0$, for example). Such a detector would be used to detect the 70 Mev Σ^0 decay photon. There is a proposal at BNL[27] to study the feasiblity of using pure CsI crystals as a high rate electromagnetic calorimeter. CsI has fast uv emission with decay constants of 10 and 35 ns. The light output, with a suitable waveshifter, is 20% that of $NaI(Tl)$ and twice that of BGO. This, in conjunction with moving the target upstream, may be the bestway to look for the $\gamma\Sigma^0$ decays. Further feasibility studies are required to evaluate this option..

D. Trigger and Particle Identification

The trigger must select events with a K^+ in coincidence with the Λ decaying into $p\pi^-$. As we have seen from the simulation, we do not want to put the γ in the trigger if we can avoid it. It is a powerful tool to reduce background, but it also reduces the

count rate. The total hadronic production rate in the target is estimated to be only of the order of 2×10^4 particles/sec so that the γ coincidence is not needed to reduce the trigger rate. Thus the first stage of the trigger would be:

Level 1 and 2 Trigger

a). signal from the Tagger,

b). two (positive) charged particles hitting the LAS T-O-F scintillator

c). one (negative) charged particle in the LAS drift chambers.

This trigger will also select the reaction

$$\gamma p \rightarrow \pi^+ p \pi^- \tag{9}$$

Thus the trigger must discriminate against such events. From FASTMC simulation studies we find that the K^+ and proton are limited to less than 60^0 and the π^- is less than 0.4 GeV/c. See Figures 11 and 12. Thus higher level trigger cuts to impose would be

Level 3 Trigger

d). $\theta \leq 60^0$ for the positive charged particles

e). $P < 0.5 GeV$ for the negative charged particle.

Finally to select a K^+,

Level 4 Trigger

f). The T-O-F vs. P of one of the positive charged particles should be consistent with a kaon.

Since the kaon momentum of interest is less than 1.5 GeV/c, this will be an effective off-line cut, (except for accidentals), but how effective an on-line cut it will be will depend on the on trigger momentum resolution. Figure 13 shows the T-O-F versus momentum plot for kaons and π^+ from the reactions

$$\gamma p \rightarrow K^+ Y^- \tag{10}$$

and

$$\gamma p \rightarrow \pi^+ p \pi^- \tag{11}$$

There is a clear separation for these reactions, which will give good π^+-kaon separation. Note that it might be possible to add a T-O-F greater than $15ns.$ cut to the Level 1 trigger. Figure 14 shows the background $\pi^+p\pi^-$ data, but with the beam photon shifted by two nanoseconds. Clearly some accidentals will satisfy the trigger.

The estimated trigger rates/sec are given in Table VI, for the conditions listed in the count rate section. The $\gamma p \rightarrow K^+Y^-$ trigger rates have the various branching ratios folded in. The reaction $\gamma p \rightarrow \pi^+p\pi^-$ has an average cross section of about 45 μb in the energy range of tagged photons, $(1.7 - 2.2 GeV)$. The trigger rate for these events are also given in the table. Finally the trigger rates for this reaction from untagged photons is given. In this calculation it was assumed that the accidental rate for a untagged photon to give a $\pi^+p\pi^-$ event $2ns.$ out of time is 1/50 of the true rate for a beam of 10^7 $\gamma/sec.$ Further, it was assumed that the Level 4 trigger would eliminate one half of these events, and more than 90% of the true $\gamma p \rightarrow \pi^+p\pi^-$ events. As can be seen from the table, the trigger rates are quite modest.

We have used a file of $\gamma p \rightarrow \pi^+p\pi^-$ events as input to the FASTMC program to estimate the number of reconstructed Y^*'s and Λ's due to π^+'s which are misidentified as kaons. For the small sample run to date, (equivalent to about one hour of beam time, for $N_\gamma = 10^7$ γ/sec) only 20 events survived the mass cuts and the trigger Level 3 cuts. No events satisfied the photon missing mass cuts. Further simulation is needed to verify this result.

IV. Beam Time Request

Setup and calibration will take place during the setup and calibration runs for Ref. 23. These numbers include the usual 50% data-taking efficiency.

Trigger studies	50 hours
$E_e = 3.2$ GeV	200 hours
$E_e = 2.4$ GeV	1000 hours

The count rates shown in Table Va indicate that although 100 hours of running at $E_\gamma = 3.2$ GeV would give a good measurement of the $\Lambda(1520) \rightarrow \gamma\Lambda$ branching ratio, little else would be measured. Therefore we will assume that the count rate has been increased a factor of five by moving the target upstream and increasing the beam to 3×10^7 $\gamma/sec.$ As mentioned earlier this may require a fast vertex detector to reduce the

accidentals. This target position will also be compatable with Ref. 23. Then 100 hours of running at 3.2 GeV and 500 hours running at 2.4 GeV, will give the measurement shown in Table Vb. Additional data on the $\Lambda(1405)$ and $\Sigma^0(1385)$ branching ratios may be collected as an alternate trigger during the running of the "Electromagnetic Production of Hyperons" experiment. However, they will be running at a lower energy, 1.8 GeV, which will give low count rates for the radiative decay measurement. We assume that the shower counter will have been calibrated in earlier experiments and that this information will be available at beam time.

Further studies on the feasibility of increasing the $\gamma\Sigma^0$ branching ratio signal thru the use of small, good energy backangle photon detector will continue.

V. Equipment Request

This experiment would require the following resources from CEBAF

1. Tagged photon beam
   Flux $1 - 3 \times 10^7\ \gamma/sec$
   Energy resolution $\Delta E_\gamma/E_\gamma = 0.25\% FWHM$ for a 20% energy bite
2. LAS Spectrometer as proposed in CDR
3. Shower Counter with at least 45^0 coverage. (90^0 coverage preferable).
4. Liquid hydrogen target 15 cm long, thin walled.
5. Data acquisition system as proposed in the CDR

Possible equipment to be provided by the experimenters

1. Scintillating fiber vertex detector.
2. Small good energy resolution back angle photon detector.

VI. Collaboration

Rice University and The College of William and Mary will take primary responsiblity for this phase of the hyperon experiments. Although this proposal has not been joined with that of Carnegie Mellon University, Catholic University of America, Los Alamos National Laboratory, Virginia Polytechnic Institute and State University, CE-

BAF, and Florida State University group's proposal, "Electromagnetic Production of Hyperons," (R. Schumacher, Spokesman), it is clearly in the interests of our group to do so in the near future.

VII. References

1. T. Goldman, LAMPF II Workshop Report 1982 (unpublished) and M.V. Hynes' FNAL Letter of Intent, "Primakoff Production at Hyperon Exicted States" (unpublished).

2. D. A. Whitehouse *et al.*, Phys. Rev. Lett. **63**, 1352 (1989); B. L. Roberts *et al.*, "Radiative Kaon Capture and Hyperon Excited States," BNL Proposal E-811 (1985).

3. R. Bertini *et al.*, PANIC 10, Heidelberg 1984 (unpublished), contributed paper M18. These data have not been subsequently published.

4. J. Lowe *et al.*, Nucl. Phys. **B209**, 16 (1982).

5. J. Darewych, M. Horbatsch, and R. Koniuk, Phys. Rev. **D28**, 1115 (1983).

6. E. Moniz, M. Soyeur, and T. Kaxiras; and T. Kaxiras, see Refs. 1 and 2.

7. J. Darewych, R. Koniuk, and N. Isgur, Phys. Rev. **D32**, 1765 (1985).

8. Y. L. Zhong, A. W. Thomas, B. K. Jennings, and R. C. Barrett, Phys. Rev. **D38**, 837 (1988).

9. H. Burkhardt, J. Lowe, and A. S. Rosenthal, Nucl. Phys. **A440**, 653 (1985).

10. R. L. Workman and H. W. Fearing, Phys. Rev. **D37**, 3117 (1988).

11. R. H. Dalitz and S. F. Tuan, Ann. Phys. (NY) **10**, 303 (2960).

12. N. Isgua and G. Karl, Phys. Rev. **D18**, 4187 (1978); **D19**, 2653 (1979); **D20**, 1191 (1979); **D22**, 1 (1982); K. Maltman and N. Isgur, Phys. Rev. **D34**, 1372 (1986).

13. Veit *et al.* Phys. Rev. **D31**, 1022 (1985); **D31**, 2242 (1985).

14. R. Koniuk and N. Isgur, Phys. Rev. **D21**, 1868 (1980); K. T. Chad, N. Isgur, and G. Karl, Phys. Rev. **D23**, 155 (1981).

15. D. Strottman, Phys. Rev. **18**, 2716 (1978).

16. F. Dydak *et al.*, Nucl. Phys. **B118**, 1 (1977).

17. T. S. Mast *et al.*, Phys. Rev. Lett. **21**, 1715 (1968).

18. J. Colas *et al.*, Nucl. Phys. **B91**, 253 (1975).

19. W. Humphreys and R. Ross, Phys. Rev. **127**, 1305 (1962).

20. J. D. Davies *et al.*, Nucl. Physl **B160**, 492 (1979).

21. B. Mecking, "A Large Acceptance Magnetic Spectrometer for CEBAF," (CEBAF internal report).

22. E. L. Smith, "Fast Monte Carlo Program for the CLAS Detector CLAS-NOTE-89-009.

23. P. Barnes *et al.*, CEBAF Proposal "Electromagnetic Production of Hyperons," unpublished.

24. D. Joyce, "CELEG-CEBAF Large Acceptance Spectrometer Event Generator, CLAS-NOTE-89-004.

25. D. P. Barber *et al.*, Z. Physik **C7**, 17 (1980).

26. A. M. Boyarski *et al.*, Phys. Lett. **34B**, 547 (1971).

27. C. L. Woody *et al.* "Proposal to Study Large Pure *CsI* Crystals in a Potential High Resolution Electromagnetic Calorimeter for RHIC," *private communication.*

TABLE I

Calculated Raditive Widths Γ_γ (keV)

Transition	MIT Bag[6]	IK-SU(6)[6]	IK-uds[6]	DHK[7]
$\Lambda(1520) \to \Sigma(1385)$	0	0.034	0.079	~0
$\Lambda(1520) \to \Sigma(1193)$	3.4	49	45	74
$\Lambda(1520) \to \Lambda(1405)$	0.002	0.35	0.66	0.2
$\Lambda(1520) \to \Lambda(1116)$	0.8	88	122	96
$\Lambda(1405) \to \Sigma(1385)$	0	0.24	0.23	0.3
$\Lambda(1405) \to \Sigma(1193)$	0	65	60	91
$\Lambda(1405) \to \Lambda(1116)$	2.8	137	164	143
$\Sigma(1385) \to \Sigma(1193)$	14	19	19	19
$\Sigma(1385) \to \Lambda(1116)$	154	243	242	232

TABLE II

Branching Ratios for $K^- p \to \Lambda\gamma$, $\Sigma^0\gamma$ in Units of 10^{-3}

NRQM = Nonrelativistic Quark Model
CBM = Cloudy Bag Model

Theory	$R_{\Lambda\gamma}$	$R_{\Sigma^0\gamma}$
NRQM[7]	3.4	2.6
CBM[8]	1.9	2.3
Data		
Ref. 2	$0.86\pm0.07^{+0}_{-0}{}^{.10}_{.08}$	$1.44\pm0.20^{+0}_{-0}{}^{.12}_{.10}$
Ref. 4	2.8 ± 0.8	
Ref. 19	3.0 ± 1.5	
Ref. 20		<4

TABLE III

ASSUMED SYSTEM PARAMETERS

All values as listed in CDR unless otherwise noted.

a) Magnetic Field	
i) Negative particles bend away from axis	
ii) $B=0.2 \cdot B$	
b) Threshold Cuts	$p_\pi > 50$ MeV/c
c) Momentum Resolution	$\Delta p = \Delta p/0.2$
d) Angular resolution	unchanged
e) Shower Counter - Coverage to 45°	
Energy resolution	$\sigma_E = 10\%/\sqrt{E}$
Position Resolution	$\sigma_x = 2.0$ cm$/\sqrt{E}$
f) Tagged Photon Beam N_γ/sec	10^7 γ/sec
Resolution	$\Delta E_\gamma = 5$ MeV
Range	0.7-0.9 E_e
Electron Energy	2.4 GeV

TABLE IV

Hyperon Parameters and Branching Ratios

$\Sigma^0(1385)$	M_Σ=1384 MeV		Γ=36 MeV	
R_1	Mode		R_2	Mode
0.877**	$\pi^0\Lambda$			
0.12	$\pi\Sigma$	−	0.50	$\pi^+\Sigma^-$
			0.0	$\pi^0\Sigma^0$
			0.50	$\pi^-\Sigma^+$
0.002	$\gamma\Lambda$			
0.001	$\gamma\Sigma^0$			

$\Lambda^*(1405)$	M_Λ=1405 MeV		Γ=40 MeV	
0.997*,**	$\pi\Sigma$	−	0.50	$\pi^+\Sigma^-$
			0.33	$\pi^0\Sigma^0$
			0.17	$\pi^-\Sigma^+$
0.001	$\gamma\Lambda$			
0.002	$\gamma\Sigma^0$			

$\Lambda(1520)$	M_Λ=1520 MeV		Γ=16 MeV	
0.45	$N\bar{K}$			
0.42	$\pi\Sigma$	−	0.50	$\pi^+\Sigma^-$
			0.33	$\pi^0\Sigma^0$
			0.17	$\pi^-\Sigma^+$
0.11	$\pi\Sigma^{**}$	−	0.50	$\pi^+\Sigma^-$
			0.33	$\pi^0\Sigma^0$
			0.17	$\pi^-\Sigma^+$
0.01	$\gamma\Lambda$			
0.01	$\gamma\Sigma^0$			

*Above M_Λ=1432 MeV ($N\bar{K}$ threshold): R_1=0.45, Mode=$N\bar{K}$

**Below M=1330 MeV ($\pi\Sigma^0$ threshold): Mode=$N\pi$

TABLE Va.

Estimated Count Rate and Backgrounds for 10^7 γ/sec

Decay	Particle Detected	Counts/100 hrs	Background
$\Lambda(1520)\rightarrow\gamma\Lambda$	$K^+p\pi^-$	400	20 ($\gamma\Sigma^0$)
	$\gamma K^+p\pi^-$	130	0
$\Lambda(1520)\rightarrow\gamma\Sigma^0$	$\gamma K^+p\pi^-$	80	25 ($\pi^0\Sigma^0$)
	$2\gamma K^+p\pi^-$	12	2 ($\pi^0\Sigma^0$)
$\Lambda(1405)+\Sigma(1385)\rightarrow\gamma\Lambda$	$K^+p\pi^-$	45	5 ($\gamma\Sigma^0$)
	$\gamma K^+p\pi^-$	12	0
$\Lambda(1405)+\Sigma(1385)\rightarrow\gamma\Sigma^0$	$\gamma K^+p\pi^-$	---	---
	$2\gamma K^+p\pi^-$	10	2 ($\pi^0\Sigma^0$)

TABLE Vb

Estimated Count Rate for Target 50 cm Upstream and $N_\gamma=3\times10^7$ γ/sec

Decay	Particle Detected	Counts/100 hrs	Background
$\Lambda(1520)\rightarrow\gamma\Lambda$	$\gamma K^+p\pi^-$	650	~0
$\Lambda(1520)\rightarrow\gamma\Sigma^0$	$\gamma K^+p\pi^-$	400	125 ($\pi^0\Sigma^0$)
	$2\gamma K^+p\pi^-$	60	10 ($\pi^0\Sigma^0$)

Decay	Particle Detected	Counts/500 hrs	Background
$\Lambda(1405)+\Sigma(1385)\rightarrow\gamma\Lambda$	$K^+p\pi^-$	1100	125 ($\gamma\Sigma^0$)
	$\gamma K^+p\pi^-$	300	~0
$\Lambda(1405)+\Sigma(1385)\rightarrow\gamma\Sigma^0$	$2\gamma K^+p\pi^-$	200	50 ($\pi^0\Sigma^0$)

TABLE VI : TRIGGER RATES

E_γ Range (GeV)	Reaction	$\sigma(\mu b)$	$N_\gamma (\times 10^7)$	3 Charged x LAS Acceptance	Level I Triggers/sec	Level III Triggers/sec	Level IV Triggers/sec
1.7 - 2.2	$\gamma p \to K^+ Y$	5	1.0	0.047	1.4	1.4	1.4
1.7 - 2.2	$\gamma p \to N\pi\pi$	45	1.0	0.054	15.0	3.5	<1
	ACCIDENTALS (1/50 of Events Seen for N_γ = 1 x 10^7 γ/sec)						
1.7 - 2.2	$\gamma p \to N\pi\pi$	45	0.7	0.054	0.2	0.05	---
1.3 - 1.8	$\gamma p \to N\pi\pi$	125	1.8	0.056	1.5	0.42	~0.2
0.9 - 1.4	$\gamma p \to N\pi\pi$	450	2.1	0.046	5.2	2.16	~1
	Total trigger rate for N_γ = 1 x 10^7 γ/sec				23.3	7.5	~3
	Total trigger rate for N_γ = 3 x 10^7 γ/sec				78.5	38.4	~17

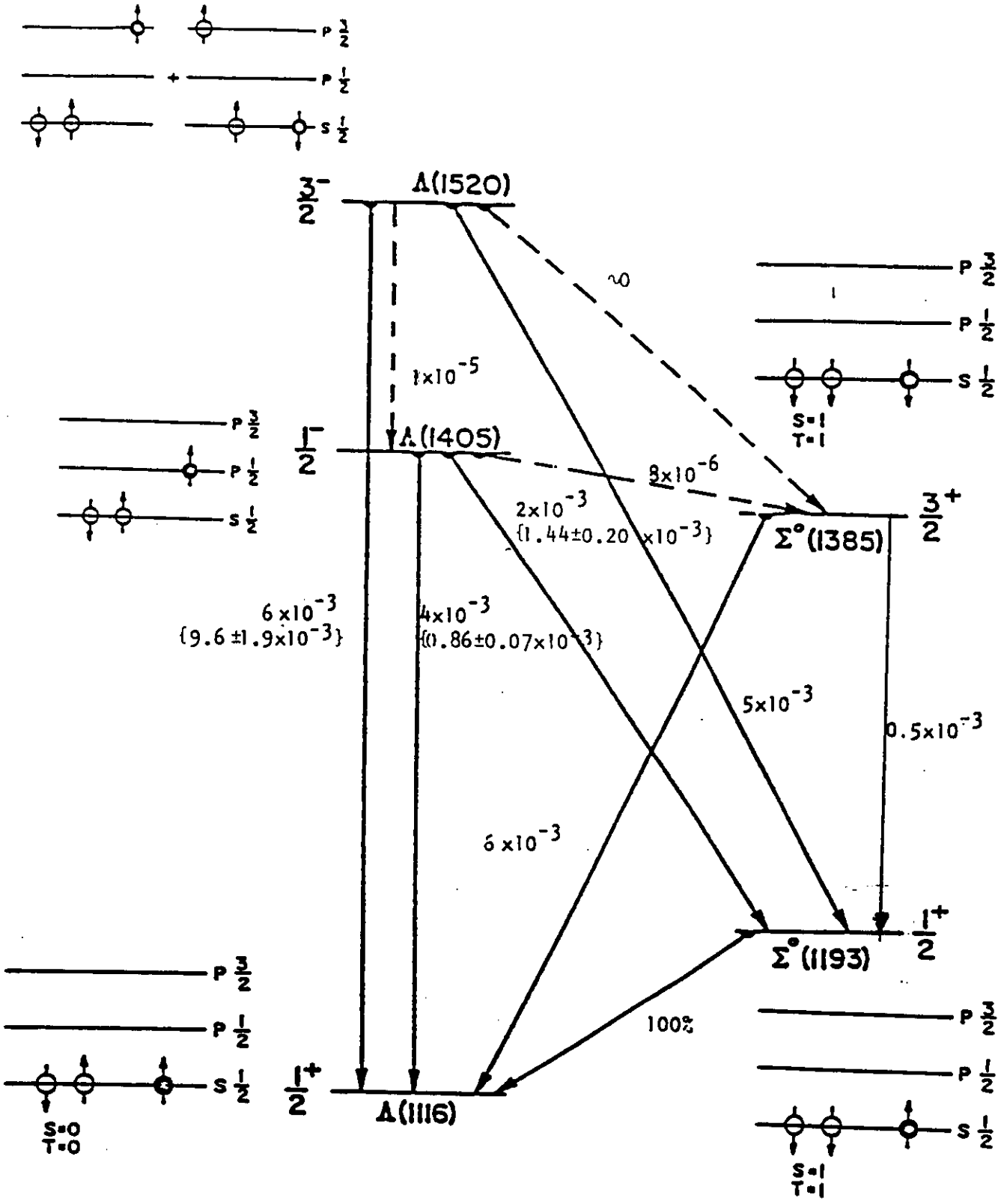

Figure 1: **$\Lambda^*(1520)$ radiative decay scheme**
The branching ratios were calculated using the NROM[6]. The experimental values are given in Refs. 2 and 17, and noted in brackets above.

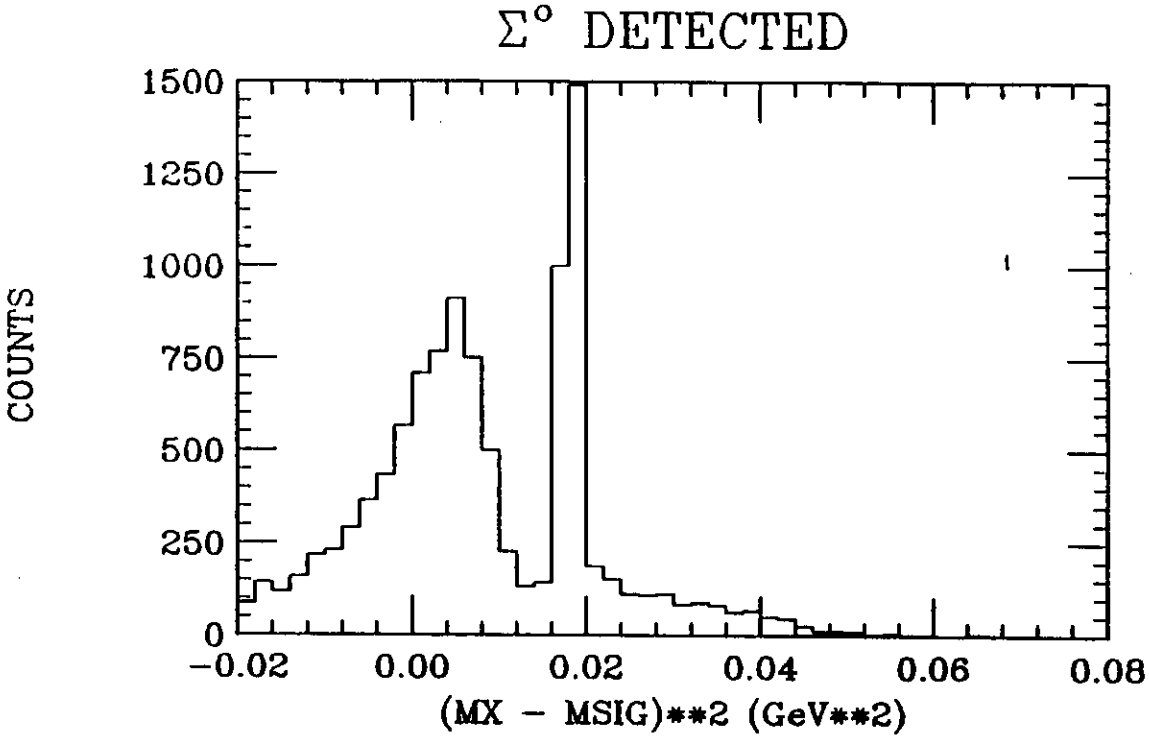

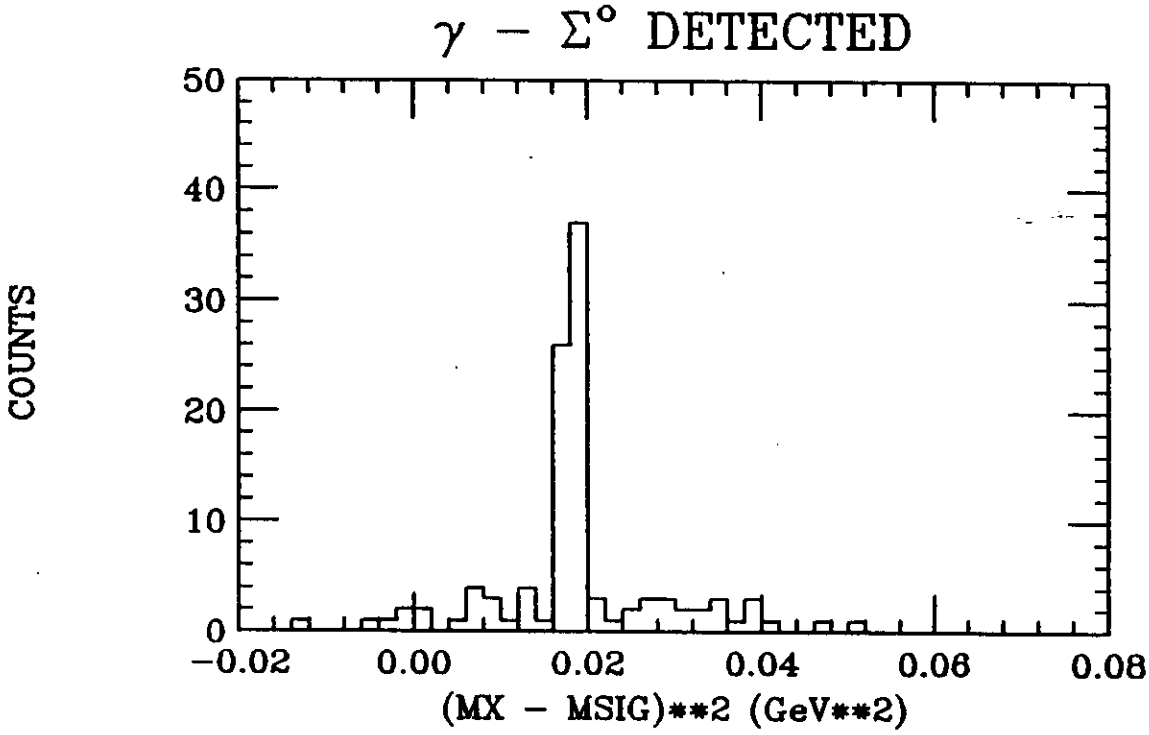

Figure 9: Missing mass spectrum of photon from reaction $\gamma p \rightarrow K^{+}\Lambda(1405), \Sigma(1385) \rightarrow K^{+}\gamma\Sigma^{0}$

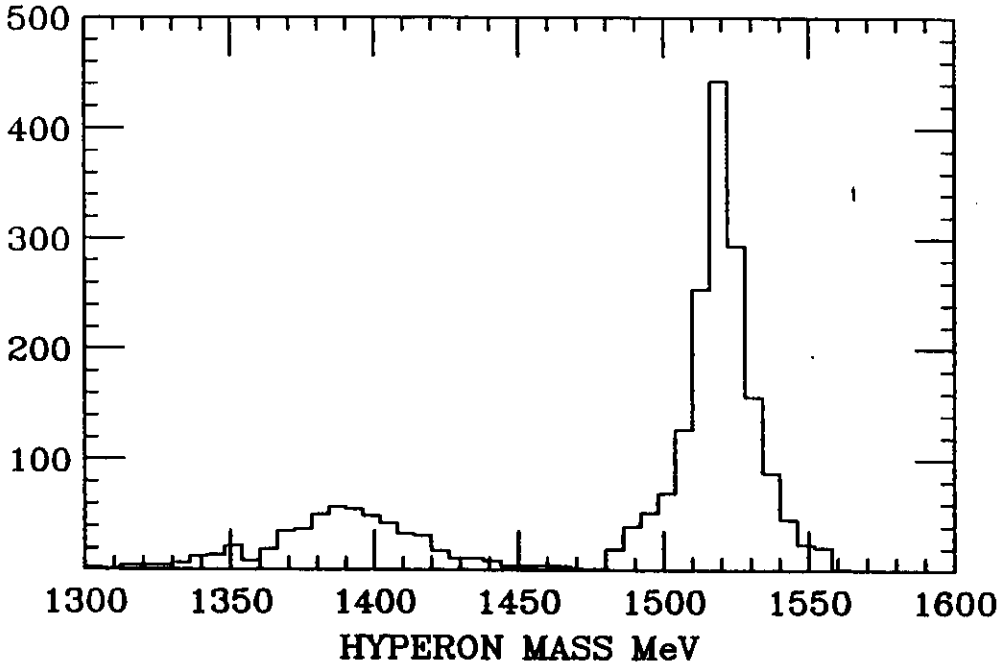

Figure 10a: Hyperon mass plot for 500 hours of data for $N_\gamma = 10^7$ γ/sec

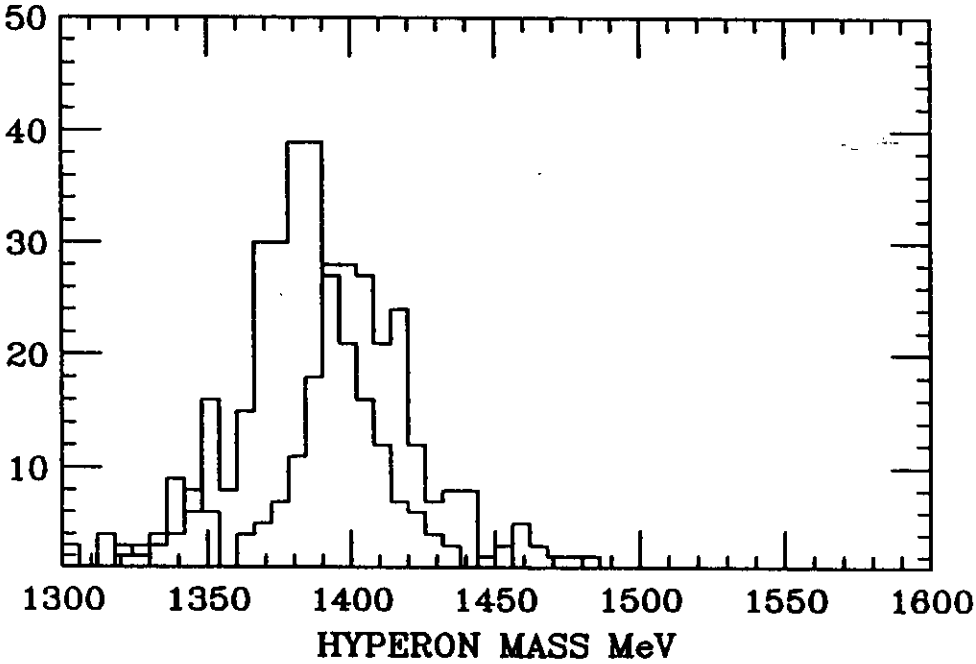

Figure 10b: Λ(1405) mass and Σ(1385) mass for 500 hours of data for $N_\gamma = 10^7$ γ/sec

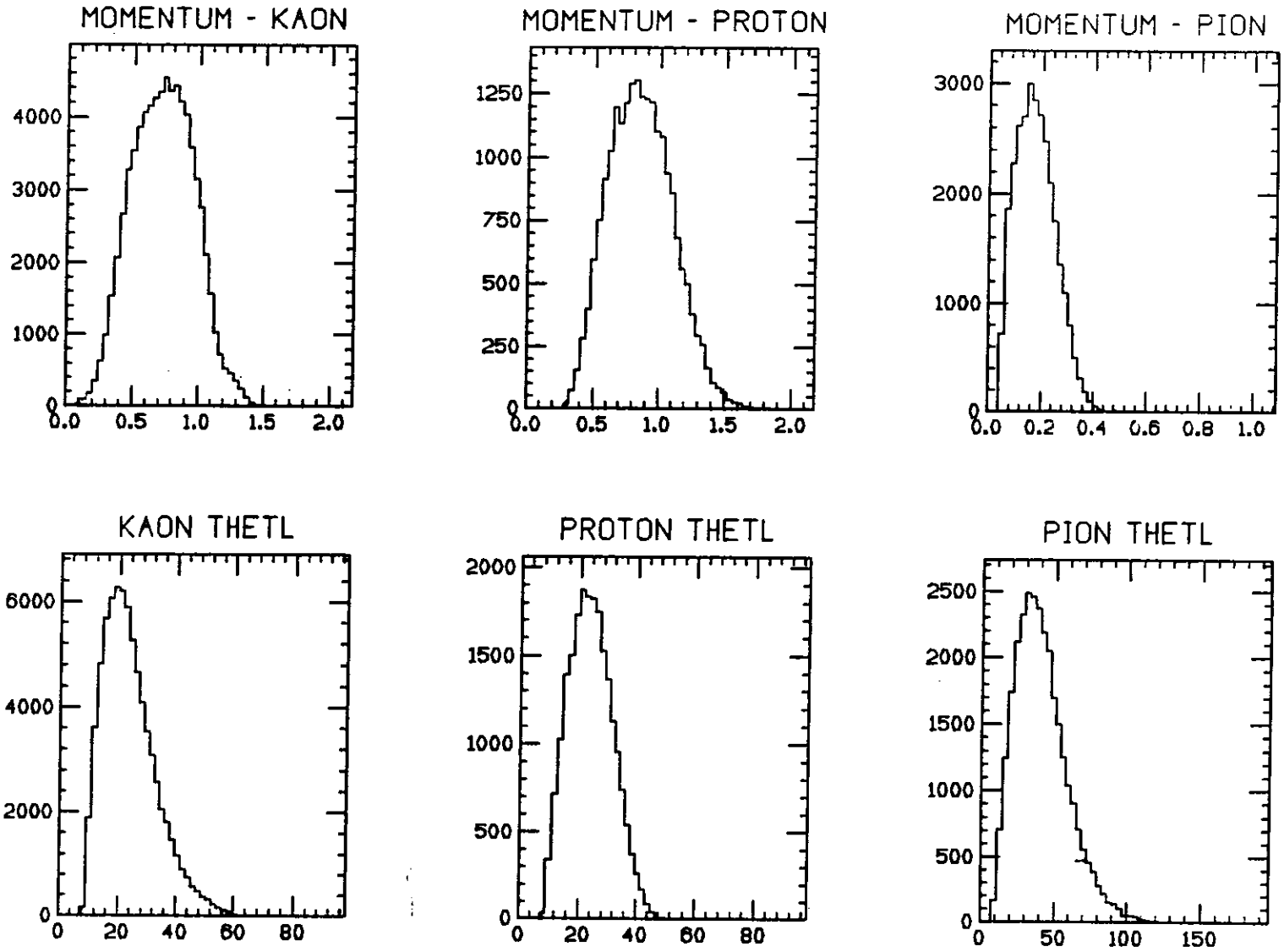

Figure 11: Kaon, proton, and π^- laboratory momentum and angles for reaction $\gamma p \rightarrow K^+ \Lambda(1405)$, $\Sigma(1385)$

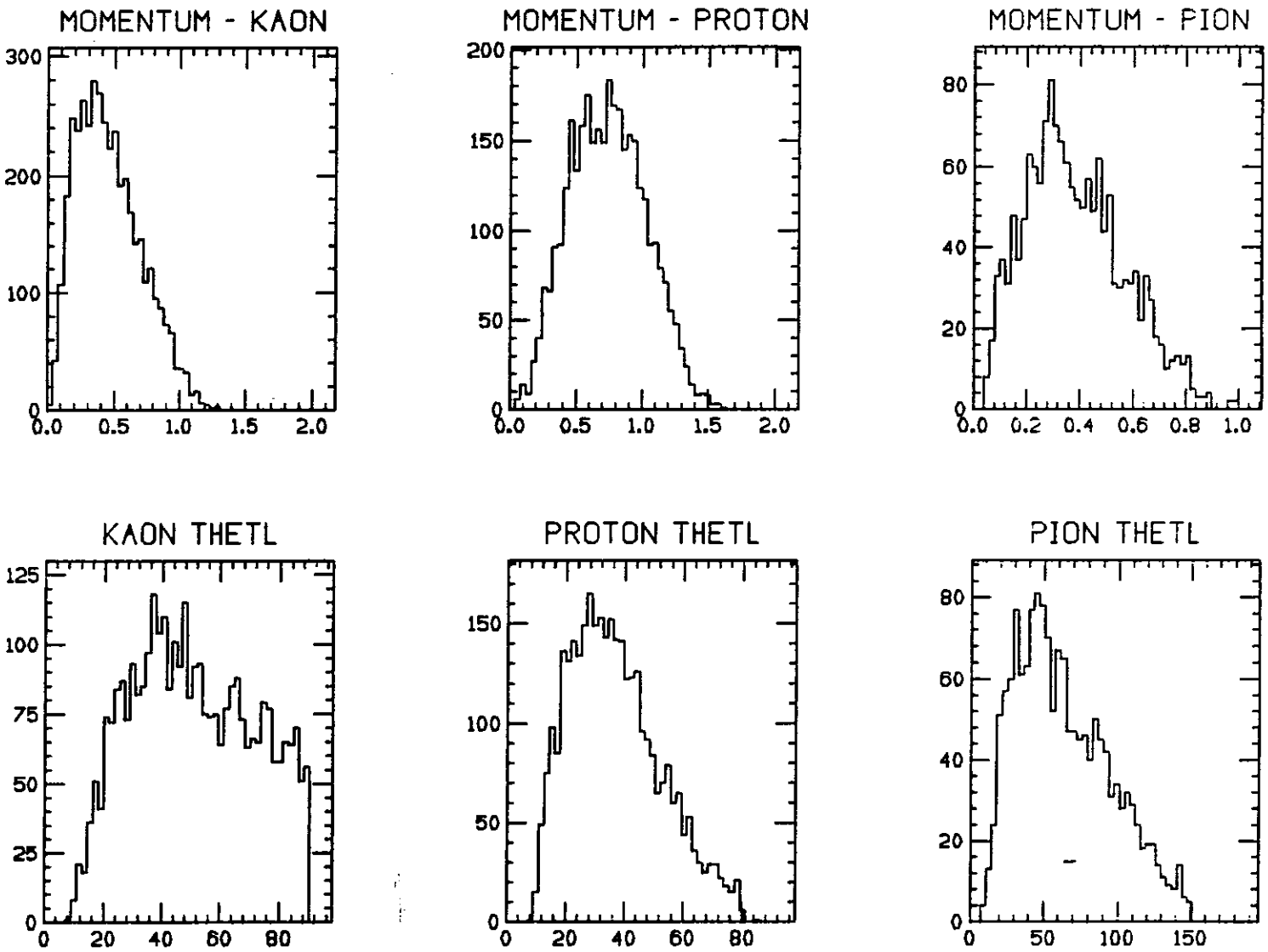

Figure 12: Kaon (actually π^+ misidentified) proton and π^- laboratory momentum and angles for reaction $\gamma p \to \pi^+ p \pi^-$ (E_γ=1.0-1.4 GeV)

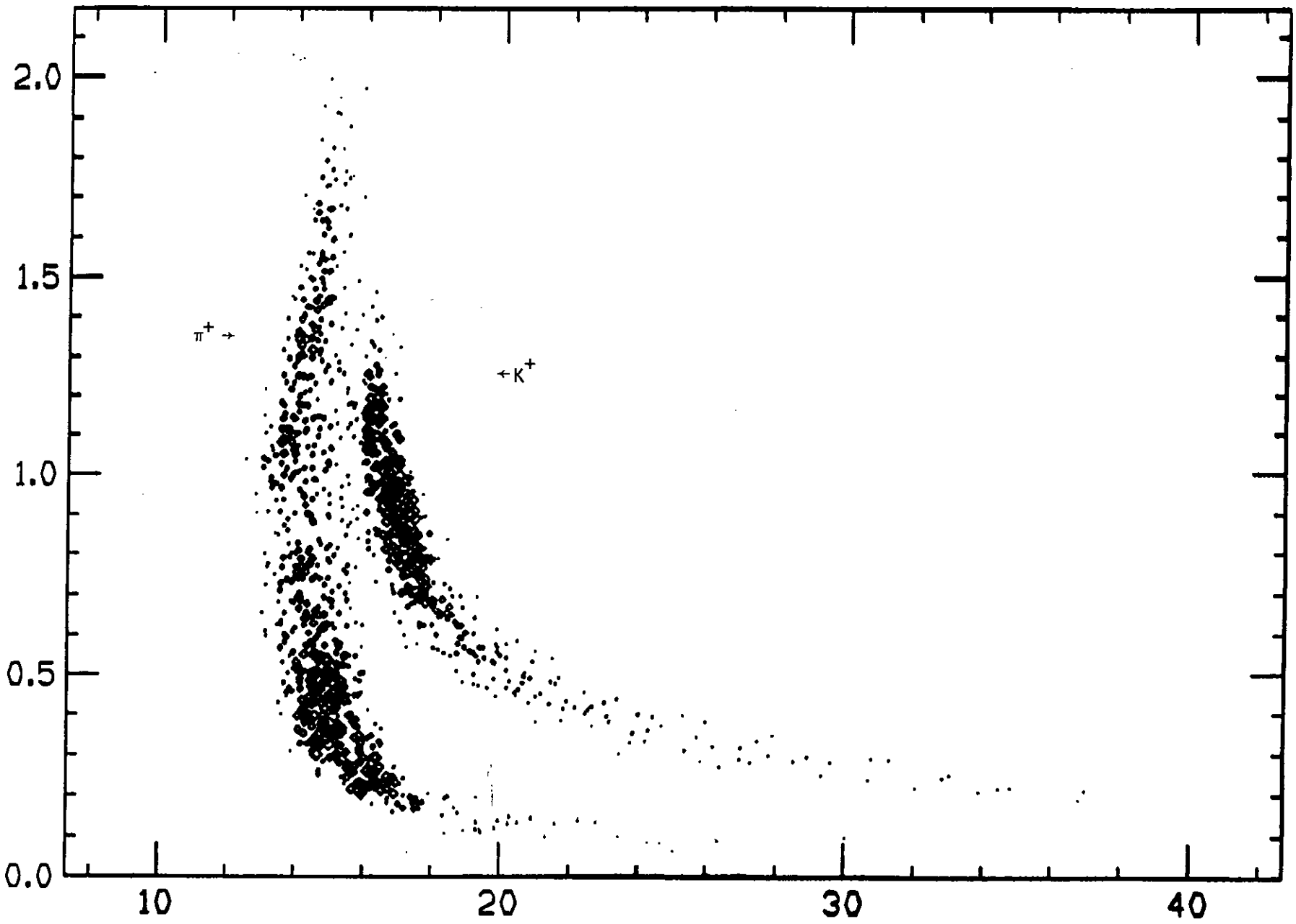
T-O-F VS. P FOR KAON
2.0
1.5
1.0
0.5
0.0
10
20
30
40
π+ →
← K+

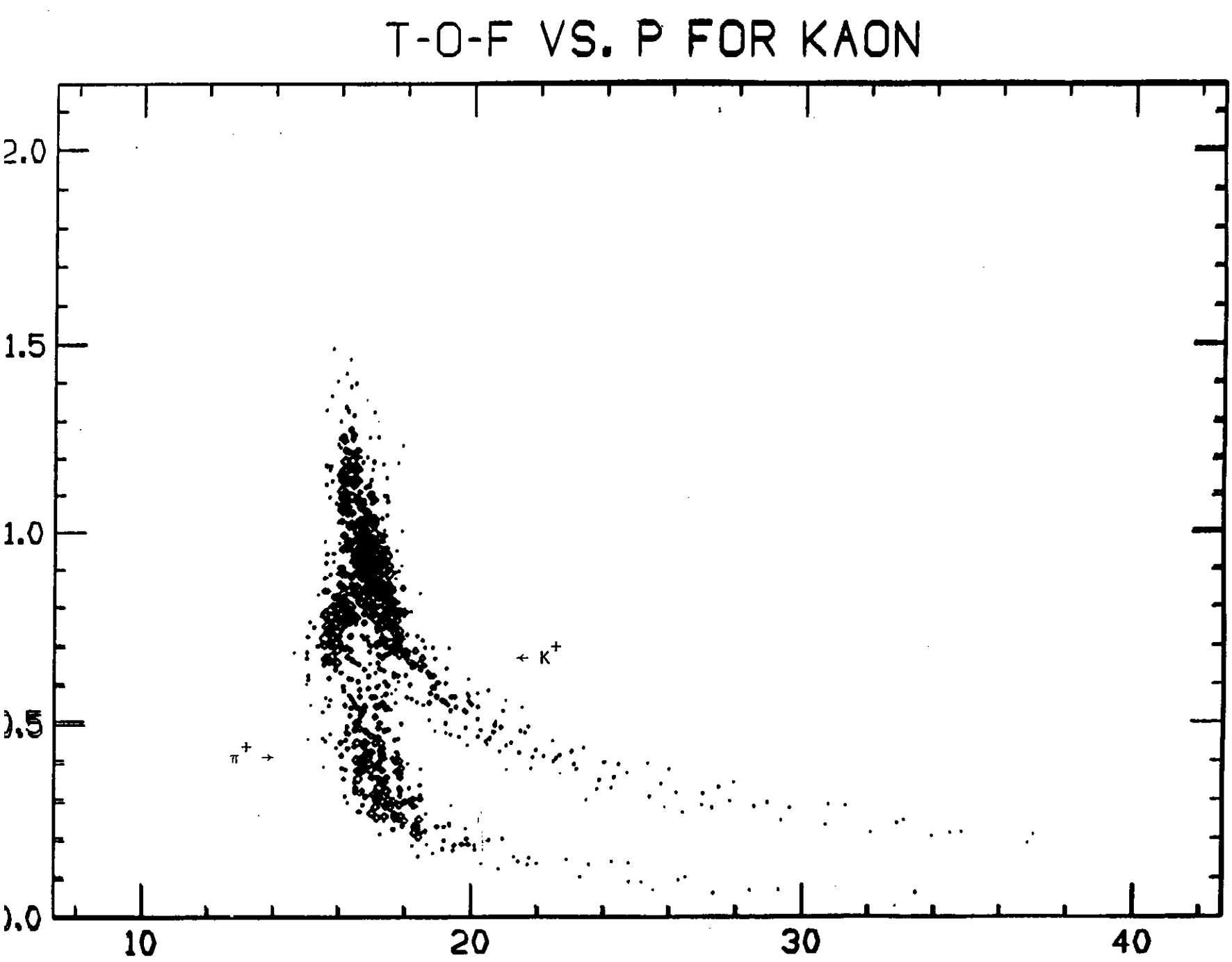

Figure 14: T-O-F vs. momentum for K^+ and π^+ delayed by 2 nanoseconds.

APPENDIX

HYPERON DECAYS

by

T. Goldman, M. V. Hynes, R. E. Mischke, and T. Oka
Los Alamos National Laboratory

T. W. L. Sanford
Sandia National Laboratory

Just as LAMPF has permitted new levels of precision in investigations involving pions and muons, LAMPF II will facilitate such progress above the threshold for production of particles with strangeness. While the strange mesons may receive most attention from particle physicists, the strange baryons also provide essential input to the search for a complete description of subatomic physics. To keep the discussion of hyperon decays together, some topics in strong-interaction physics are included in addition to those relevant to electroweak physics. Hyperon-nucleon interactions are discussed in a separate section of this document.

I. PRODUCTION OF HYPERONS

The high fluxes of mesons at LAMPF II will favor hyperon production by π's and K's over that by the primary proton beam. The strong-interaction physics to be learned from the production mechanism will involve both kinds of beams. Particularly interesting has been the discovery of polarization of hyperons produced with moderate transverse momentum.[1,2] The data show that Λ's, Ξ^0's, and Ξ^-'s are polarized and Σ^+ are produced polarized with the opposite sign. $\bar{\Lambda}$'s are unpolarized. The polarization versus transverse momentum is basically independent of target and incident energy (for comparable Feynman x values).

These data have had considerable impact on models of hyperon production. For instance, thermodynamic models do not predict polarization, and in QCD models with many contributing diagrams polarization is unlikely. Quark models[3] have had some success in describing the observations and a next generation of experiments will provide input for refining these models. While the region of highest transverse momentum will be probed at Fermilab, systematic experiments, at lower energies will be very important. At LAMPF II energies, final-state multiplicities are manageable, which will facilitate the study of exclusive channels.

II. HYPERON STRUCTURE

Many of the hyperon ground-state properties have been measured already to good precision at existing facilities. Indeed, even the excited-state spectra of the Λ, Σ, and Ξ have been known for some time. Yet the crucial data addressing the issue of hyperon structure in terms of the quark model are missing. The status of our understanding of baryon structure in general and hyperon structure in particular is similar in many ways to early developing stages of the nuclear shell model (about 1950). At that time there was an abundance of models each equally successful in reproducing the ground-state properties and excited-state spectra of nuclei. Yet each model made very different predictions for the structure present in these states. The same diversity in structure is present today in the various quark model predictions for the baryons.[4] Just as in nuclei, measurements of electromagnetic decays of baryon excited states will test our quark model understanding with the high precision unique to electromagnetic processes.

In a simple three-quark model (q^3), the ground states of the Λ, Σ, and Ξ have up, down, and

strange quarks in the S1/2 orbit. The light quarks (up and down) are coupled to total spin-isospin S = 0, T = 0 for the Λ and to S = 1, T = 1 for the Σ as displayed in Fig. 1. The remaining S = -1 even-parity state, Σ*(1385)3/2⁺, has the strange quark spin aligned with the S = 1, T = 1 light quarks (Fig. 1). The ground and excited states of the Ξ have two strange quarks in the S1/2 orbit coupled to S = 1 as shown in Fig. 2. For the ground state the remaining light quark is in the S1/2 orbit coupled to give S = 1/2, T = 1/2, whereas for the excited state it is coupled to give S = 3/2, T = 1/2.

The odd-parity states, Λ*(1405)1/2⁻ and Λ*(1520)3/2⁻, have one quark in the P1/2 and P3/2 orbits, respectively. DeGrand and Jaffe[4] have pointed out that the kinetic energy for the 1/2⁻ state is considerably lower if the strange quark, rather than one of the light quarks, is placed in the P1/2 level. Thus the q^3 S1/2 configuration for the Λ*(1405)1/2⁻ state consists of the light quarks in S1/2 coupled to S = 0, T = 0, and the strange quark in the P1/2 orbit as shown in Fig. 3. This

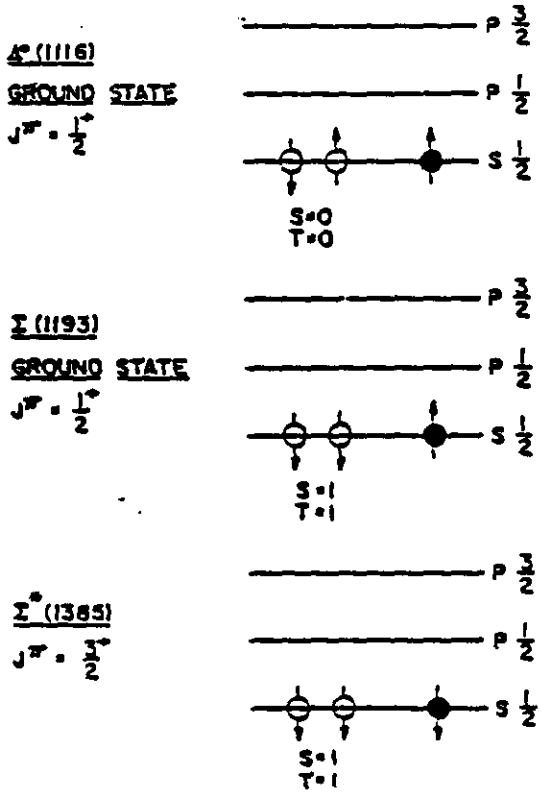

Fig. 1. Quark-level occupation diagram for the Λ,Σ ground states and for the Σ*(1385) in the q^3 model.

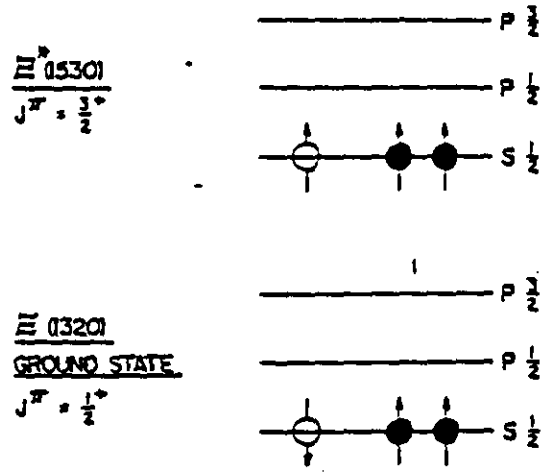

Fig. 2. Quark-level occupation diagram for the Ξ ground and excited states in the q^3 model.

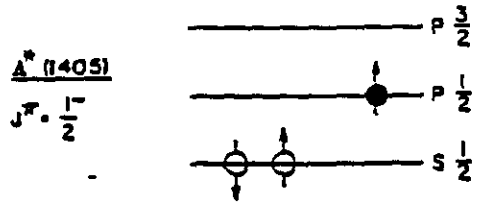

Fig. 3. Quark-level occupation diagram for the Λ*(1405) in the q^3 model.

configuration requires that any radiative transition from this state is a pure, strange quark P1/2 → S1/2 transition. Because the electromagnetic operators can change the quantum numbers of only one particle, the radiative widths for Λ*(1405) → Σ⁰(1193)γ, or Σ*(1385)γ, are strictly zero.

The simplest q^3 configuration assumption for the Λ*(1520)3/2⁻ has the strange quark in the P3/2 state with the light quarks coupled to S = 0, T = 0. However, gluon exchange calculations by DeGrand[5] and others indicate a sizable admixture of light quark occupation in the P3/2 orbit with the remaining quarks in S1/2 coupled to S = 0, T = 0, as shown in Fig. 1. In the notation of DeGrand, the Λ*(1520)3/2⁻ wave function is written as

$$\Lambda^*(1520)3/2^- = a\ {}^4\underline{R} + b\ {}^2\underline{R} + c\ {}^2\underline{I}$$

$$|a|^2 + |b|^2 + |c|^2 = 1 .$$

where $^{2S+1}\underline{\sigma}$ means the SU(3) flavor multiplet σ with total spin S. DeGrand finds c = 0.85, b = -0.51, a = 0.1, indicating a predominance of singlet and octet configurations as already discussed. The $^4\underline{8}$ component corresponds to having one quark in the P1/2 orbit, the two S-state quarks coupled to S = 1, and the system coupled to $J/2^-$. Other gluon exchange calculations find similar admixture coefficients with smaller $^4\underline{8}$ contributions, however. If the small $^4\underline{8}$ admixtures are ignored, the wave function is as shown in Fig. 4. This configuration and the one-body nature of the electromagnetic operators implies that the radiative width for the transition $\Lambda^*(1520) \to \Sigma^*(1385)\gamma$ is zero. We have therefore in the pure q^3 model three forbidden radiative transitions $\Lambda^*(1405) \to \Sigma^0(1193)\gamma$, $\Sigma^*(1385)\gamma$, and $\Lambda^*(1520) \to \Sigma^*(1385)\gamma$ due to this selection rule.

There is an additional selection rule that enters for some of the transitions of interest here. The SU(3) classification scheme places the ground states of Σ and Ξ in the $1/2^+$ baryon octet whereas their first excited states, $\Sigma^*(1385)$ and $\Xi^*(1530)$, are members of the $3/2^+$ baryon decuplet as displayed in Fig. 5. In this figure t_3 is plotted versus hypercharge with I-spin, U-spin, and V-spin axes. In pure SU(3), I-spin and U-spin are invariants. Thus the Σ^{*-} and Ξ^{*-} being in a U-spin quartet cannot decay through a U-spin scalar interaction to their respective ground states, which are in a U-spin doublet. The photon transforms as a U-spin scalar and thus the electromagnetic decay of these states to their ground states is forbidden. In contrast, the electromagnetic decays of the Σ^{*0}, Σ^{*+}, and Ξ^{*0} to their respective ground states do not violate U spin and are thus allowed.

SU(3) is, of course, a broken symmetry and it is precisely the symmetry breaking that splits the

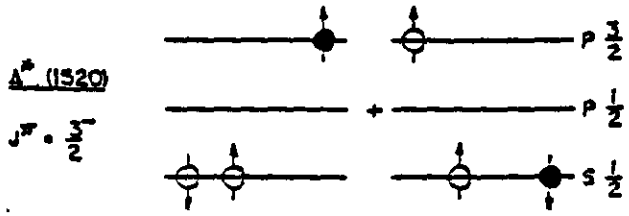

Fig. 4. Quark-level occupation diagrams for the $\Lambda^*(1520)$ in the q^3 model. Both singlet and octet configurations are shown.

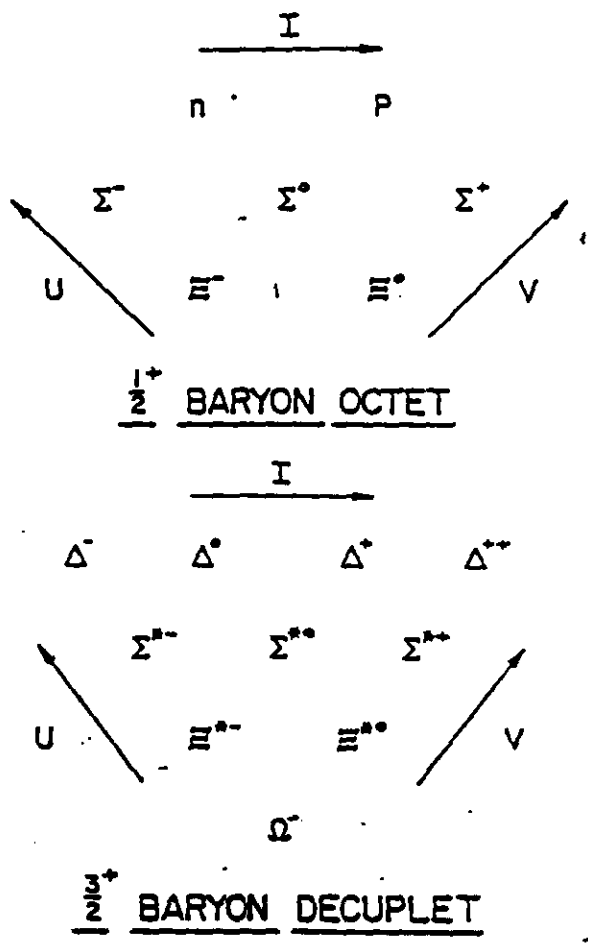

Fig. 5. t_3 versus hypercharge display of the SU(3) baryon octet and decuplet. The I-, U-, and V-spin axes are as shown.

masses of the members of a multiplet. Thus when the constituent quarks are allowed to have different masses, the strange quark being heavier than the nonstrange ones, the forbidden transitions just cited become allowed. The electromagnetic transition amplitudes will be proportional to the difference between the strange- and down-quark masses.

The remaining allowed widths can be calculated straightforwardly from the quark wave functions:

$$\Gamma_\gamma = 2k \frac{1}{2S_i + 1} \sum_{\substack{m_i m_f \\ \lambda = \pm 1}} |\langle f, m_f| \int d\underline{r}\, \hat{e}_{\underline{k}\lambda} \cdot \underline{j} e^{i\underline{k}\cdot\underline{r}} |i, m_i\rangle|^2 |\hat{e}_{\underline{k}\lambda} \cdot \underline{k} = 0, \lambda = \pm 1 \quad .$$

In this expression the current operator is given by

$$\underline{J} = e_f \gamma^\mu \underline{a} \gamma^\nu \ ,$$

with e_f the charge of the quark with flavor f; $\underline{k}$ is the photon momentum; $\gamma(\gamma^+)$ is the initial (final) quark wave function; and a is the usual electromagnetic propagator. Moniz, Soyeur, and Kaxiras* have calculated the allowed radiative widths for the neutral $S = -1$ states of interest in the context of the fixed radius, static cavity approximation to the MIT bag model. Their results for the pure q^3 wave functions are listed in Table I. Also listed in the table are the results of T. Kaxiras,** who has calculated these widths in the context of the Isgur-Karl (IK) model.[5] In this model two sets of basis states were used. In the "SU(6)" basis the spin-isospin wave functions are symmetrized in all three quarks and they are given in the limit of equal masses. The transition widths are calculated, however, with differing quark masses. In the "uds" basis, the wave functions are symmetrized only with respect to the u and d quarks. The strange- and nonstrange-quark masses are treated as before. The results in these two cases are listed in the appropriate columns in the table. Evidently the three different predictions differ by as much as a factor of 60. In addition, some of the transitions forbidden in the MIT bag are allowed in the IK model.

The assumption of pure q^3 configurations for these states has recently been brought into question by Mulders,* who calculated the importance of $q^4\bar{q}$ admixtures for the $\Lambda^*(1405)$. In this work the quarks for the $q^4\bar{q}$ configuration were taken to be in the S1/2 orbit and the q^3 configuration was taken to be as shown in Fig. 3. Using a simple two-state mixing model, an estimate of the relative strengths was obtained.

$$\Lambda^*(1405) = 0.8\,|q^4\bar{q}\rangle \pm 0.6\,|q^3\rangle \ .$$

Such a large $q^4\bar{q}$ admixture for the $\Lambda(1405)$ considerably alters the results listed in Table I. In particular, the $\Lambda^*(1405) \to \Sigma^0\gamma, \Sigma^+\gamma$ transition rates are no longer zero. Moniz and Soyeur have calculated the effect of including these $q^4\bar{q}$ admixtures on the radiative widths by using the results of Strottman for the $q^4\bar{q}$ components in the Λ and Σ ground states.[7] These results and their estimates for such admixtures in the $\Lambda^*(1520)$ state are listed in Table II. Because the relative phase of the $q^4\bar{q}$ and q^3 contributions is not known, the table displays the results for constructive and destructive interference. The $\Lambda^*(1405)$ radiative

*E. Moniz, M. Soyeur, and T. Kaxiras, MIT, private communication.

**T. Kaxiras, private communication.

TABLE I

RADIATIVE WIDTHS IN THE MIT BAG MODEL AND IN THE ISGUR-KARL (IK) MODEL

Transition	Γ_γ(keV) MIT Bag	IK SU(6)	IK uds
$\Lambda^*(3/2^-) \to \Sigma^*(3/2^+)$	0	0.034	0.079
$\Sigma(1/2^+)$	68	49	45
$\Lambda^*(1/2^-)$	0.002	0.35	0.66
$\Lambda(1/2^+)$	3.40	88	122
$\Lambda^*(1/2^-) \to \Sigma^*(3/2^+)$	0	0.24	0.23
$\Sigma(1/2^+)$	0	65	60
$\Lambda(1/2^+)$	2.8	137	164
$\bar{\Sigma}^{*0}(3/2^+) \to \Lambda(1/2^+)$	154	243	242
$\Sigma^0(1/2^+)$	14	19	19
$\Sigma^{*-}(3/2^+) \to \Sigma^-(1/2^+)$	—	2.3	2.1
$\Sigma^{*+}(3/2^+) \to \Sigma^+(1/2^+)$	—	103	103
$\Sigma^0(1/2^+) \to \Lambda(1/2^+)$	4.30	8.4	8.8
$\Xi^{*0}(3/2^+) \to \Xi^0(1/2^+)$	—	118	119
$\Xi^{*-}(3/2^+) \to \Xi^-(1/2^+)$	—	2.6	2.8

*P. Mulders, MIT, private communications.

TABLE II

RADIATIVE WIDTHS IN THE MIT BAG MODEL FOR $q^4\bar{q}$ AND q^3 ADMIXTURES

Transition	Γ(keV) $\lvert q^4\bar{q}\rangle + \lvert q^3\rangle$	$\lvert q^4\bar{q}\rangle - \lvert q^3\rangle$
$\Lambda^*(3/2^-) \to \Sigma(1/2^+)$	100	88
$\Lambda(1/2^+)$	25	9
$\Lambda^*(1/2^-) \to \Sigma(1/2^+)$	325	325
$\Lambda(1/2^+)$	20	6

decay to the Σ ground state has no q^3 component and goes only through the $q^4\bar{q}$ admixtures.

The available electromagnetic data on the states of interest here is quite sparse. The $\Sigma^0(1193)$ decays 100% to $\Lambda^0(1116)\gamma$ and has been measured by Dydak et al.[8] to be 11.5 ± 2.6 keV. In this experiment a 20-GeV Λ beam at the CERN SPS was incident on a uranium target. The Primakoff effect was used to produce Σ^0's in the inverse reaction $\Lambda + \gamma \to \Sigma^0$. This value does not compare well with the MIT bag model calculation, which predicts 4.5 keV or about four times smaller. This is not too surprising as the same model predicts 255 keV for the $\Delta \to N\gamma$ radiative width whereas the experimental value is 630 keV. The reasons for these discrepancies are not understood. The static bag approximation neglects recoil, which will alter the theoretical predictions, but no estimate of the changed values is available. The IK model predictions, 8.4 and 8.8 keV, are about 20% low for this transition.

There exists one measurement[9] of the $\Lambda^*(1520) \to \Lambda^0(1116)\gamma$. However, to obtain the radiative width, an appreciable $\Sigma^0\gamma$ background subtraction was made assuming that the $\Lambda^*(1520)$ is an SU(3) singlet. Such a model-dependent subtraction severely compromises the utility of this measurement. Lastly, there are upper bounds on the $\Sigma^*(1385)$ radiative decay widths.[10]

The low-lying excited states of the $S = -1,-2$ baryons provide a very useful laboratory in which to study quark confinement models. The spectrum includes both positive- and negative-parity states. The positive-parity states and their interconnecting transitions allow for tests of the S-state wave functions and quark magnetic moments. In addition they may allow for tests of possible quadrupole deformations through the presence of E2 components in the transitions. The negative-parity states and their transitions provide a different test of quark wave functions, one in which the orbital quantum number of at least one quark must be changed. Finally, due to their very narrow widths, the strange-resonance excited states are ideal probes for the study of resonance propagation in nuclei. In particular a comparison of the free-space electromagnetic decays with those occurring in a nuclear medium will provide important information on the medium-modifications to confinement. An experimental determination of these radiative tr sition widths both in free space and in the nucl medium will illuminate the quark structure of th states in particular and can help to direct the velopment of quark confinement models in general

III. HYPERON DECAYS

A. Semileptonic Hyperon Decays

An understanding of weak interactions betwe quarks will come from the dynamics of high-energ collisions and from the systematics of bound states. Semileptonic decays of baryons play a c cial role in testing quark models. The present situation can be summarized by observing the suc cess of the Cabibbo theory in general, but notin several important disagreements that indicate challenges for theorists. It is likely a succes- sive approximation technique will be used—as ex- periments improve, more sophisticated models will be required until, at some point, a "correct" theory will emerge.

The comparison between theory and experiment is usually made via the six form factors that ap- pear in the general form of the hadronic weak cur rent. For semileptonic hyperon decay the Hamil- tonian is given by

$$\mathcal{H}_w = \frac{G}{\sqrt{2}} J_\lambda \ell^\lambda + \text{H.c.}$$

where $G = 10^{-5}/m_p^2$ is the usual weak-coupling con- stant,

$$\ell_\lambda = \bar{\psi}_e \gamma_\lambda (1 + \gamma_5)\psi_{\nu_e} + \bar{\psi}_\mu \gamma_\lambda (1 + \gamma_5)\psi_{\nu_\mu}$$

is the lepton current, and

$$J_\lambda = \cos\theta_1 \, \bar{u}\gamma_\lambda (1 + \gamma_5) d + \sin\theta_1 \cos\theta_3 \bar{u}\gamma_\lambda (1 + \gamma_5) s$$

is the hadronic current. The angles θ_1 and θ_3 ar from the Kobayashi-Maskawa form of the quark mixi matrix.[11] These angles must be determined from e periment.

The matrix element of the hadronic current be tween hadrons in the decay $A \to B\ell\nu$ is given by

$$\langle B|J_\lambda|A\rangle = \begin{pmatrix} \cos\theta_1 \\ \sin\theta_1\cos\theta_3 \end{pmatrix} \bar{u}_b \Big[f_1(q^2)\gamma_\lambda - i\frac{1}{m_a + m_b}\sigma_{\lambda\eta}q^\eta f_2(q^2) + i f_3(q^2) q_\lambda \frac{1}{m_a + m_b}$$

$$+ g_1(q^2)\gamma_\lambda\gamma_5 - i\frac{g_2(q^2)}{m_a + m_b}\sigma_{\lambda\eta}q^\eta\gamma_5 + i q_\lambda \frac{1}{m_a + m_b} g_3(q^2)\gamma_5 \Big] u_a \ .$$

All the form factors are relatively real by T invariance. The terms f_3 and g_2 vanish by G-parity invariance and SU(3) symmetry. The g_3 term is related to g_1 by the Goldberger-Treiman relation and for $q^2 = 0$ the relation is given by

$$g_3(0) = \frac{2m_a(m_a + m_b)}{m_K^2} g_1(0) \ .$$

This relation has not been tested by the decay, because g_3 term is multiplied by a factor $(m_e/m_a)^2$ and negligible in the electronic decay modes. However we can expect larger effect in the muonic decay modes. For example, the decay rate $\Lambda \to p\mu\bar{\nu}_\mu$ is expressed

$$\Gamma \propto \Gamma(f_1^2(0)\,(1 + 0.025a) + 0.00907\, f_1(0)f_2(0)$$

$$+ 2.986\, g_1^2(0)\,(1 + 0.046b) + 0.427\, g_1(0)g_2(0)$$

$$+ 0.00193\, g_1(0)g_3(0)$$

where

$$\Gamma = \frac{G^2 m_a^5(\sin\theta_1\cos\theta_3)^2}{12\pi^3} = 2.5542 \times 10^{-4} \ ,$$

the parameters a and r are defined as $f_1(q^2) = f_1(0)[1 + aq^2/(m_a + m_b)^2]$ and $g_1(q^2) = g_1(0)\,[1 + bq^2/(m_a + m_b)^2]$, respectively.

Using the SU(3) relation for form factors, a = 9, b = 5, and recently obtained values for F and D, that is, $f_1(0) = -1$, $f_2(0) = -\sqrt{3/2}\,\mu_p$, and $g_1(0) = -(3F + D)/\sqrt{6} = 0.865$, the ratio of $\Gamma_{G_1G_3}/\Gamma$ is

$$\frac{\Gamma_{G_1G_3}}{\Gamma} = 0.006 \ .$$

This value may be too small to obtain the information about g_3 term even in the muonic decay modes. This leaves f_1, g_1, and f_2 as the most likely to be significant.

The experimentally determined quantities are the decay rate R and angular-correlation coefficients. The lepton-neutrino angular correlation $a_{e\nu}$ (deduced from the nucleon energy spectrum) and R do not require polarized hyperons, but a_λ, a_ν, and a_p measure the correlation with the hyperon spin direction.

Explicit expressions can be written to relate R and the a's to f_1, g_1, and f_2. Experimentally, the decay rate for $\Lambda \to Ne\nu$ is related to f_1 and g_1 by

$$R = G^2\sin^2\theta\,\frac{\Delta m^5}{60\pi^3}\,(f_1^2 + 3g_1^2)(1 - 3\delta)$$

where $\Delta m = M_a - M_b$ and only terms up to first order in δ

$$\delta = \frac{\Delta m}{M_a + M_b}$$

have been kept. In addition to the rate, the magnitude of g_1/f_1 is related to the lepton-neutrino correlation coefficient $a_{e\nu}$ by [12]

$$a_{e\nu} = \frac{f_1^2 - g_1^2}{f_1^2 + 3g_1^2} - 2\delta$$

in $W(\cos\theta_{e\nu}) = (1 + a_{e\nu}\cos\theta_{e\nu})/2$. The sign of g_1/f_1 can be extracted from the correlation between the directions of the decay particles

$$a_\Sigma = \frac{2(f_1g_1 - g_1^2 - \frac{1}{3}\delta[2(f_1+g_1)^2 + 2f_2(f_1+g_1)]}{f_1^2 + 3g_1^2}$$

$$a_\Lambda = \frac{2(f_1g_1 + g_1^2) - \frac{1}{3}\delta[2(f_1-g_1)^2 + 2f_2(f_1-g_1)]}{f_1^2 + 3g_1^2}$$

$$a_p = \frac{-\frac{5}{2}f_1g_1 + \frac{5}{6}\delta[2(f_1+f_2)g_1]}{f_1^2 + 3g_1^2}$$

in $I(\hat{q}) = 1/2(1 + a_i\vec{P}_y\hat{q})$ for polarized hyperons. $\vec{P}_y$ is the hyperon polarization and $\hat{q}$ is the direction of the decay baryon.

It is also possible to specify f_1 and f_2 in terms of the electromagnetic form factors of the neutron and proton using the conserved-vector-current hypothesis. Then f_1 and f_2 are given by Clebsch-Gordon coefficients and the anomalous magnetic moments of the neutron and proton. Then g_1 is expressed in terms of two unknown SU(3) reduced form factors, F and D. Recently, Garcia and Kielanowski[13] have fit all hyperon semileptonic data to this model with F, D, and θ_1 as parameters. They assume the simpler Cabibbo theory, which just sets $\theta_3 = 0$. It is found that including radiative corrections and the q^2 dependence of the leading form factors makes a significant improvement in the fit. Even so, a few pieces of experimental data refuse to fit. Most notable is the electron asymmetry in $\Sigma^- \to n e\nu$. The sign of the ratio g_1/f_1 is opposite that predicted by the Cabibbo model.*

Only precise data on semileptonic hyperon decays will produce significant advances in theoretical understanding. It is clear that approximate SU(3) symmetry is valid and the gross features of the data are neatly catalogued. But a real theory needs to describe the symmetry-breaking effects in detail or even alternative symmetries. For example, the possibility that a left-right symmetric theory will fit the data is being investigated.

B. Nonleptonic Decays

Nonleptonic decays such as

$$\Lambda \to p\pi^0$$
$$\Sigma^- \to n\pi^-$$
$$\Xi^- \to \Lambda\pi^-$$
$$\vdots$$

are used to test the $\Delta I = 1/2$ rule and other QCD predictions.

They are transitions where the final-state baryon-pion pair can be in either a $\ell = 0$ or $\ell = 1$ state. Let s and p be the parity-changing ($\ell = 0$) and parity-conserving ($\ell = 1$) amplitudes, respectively. Then the transition matrix for hyperon decay is[14] $M = s + p(\vec{\sigma}\cdot\hat{q})$. Here $\hat{q}$ is the unit vector along the direction of the decay baryon in the hyperon rest-frame. For hadronic collisions like $\pi^- p \to \Sigma^- K^+$ the hyperon is polarized perpendicular to the plane of interaction.[15] For such a situation s and p are related to the asymmetry parameter α via

$$\alpha = \frac{2\mathrm{Re}(s^* p)}{(|s|^2 + |p|^2)}$$

in the angular distribution of the decay baryon in the hyperon frame: $I = 1 + \alpha\vec{P}_y\cdot\hat{q}$. Again $\vec{P}_y$ is the hyperon polarization.

The asymmetry parameter has been measured for many hadronic decay channels. However, the Ω^- is difficult to produce so that α is poorly known for its various decay modes. For example, Hemingway[16] measured $\alpha = -0.2 \pm 0.4$ for $\Omega^- \to \Lambda K^-$ decay. The result is in agreement with the calculation of Finjord,[17] who expects the decay to be nearly parity conserving. Statistics are weak, however, so much could be learned by increased Ω^- production at LAMPF II.

Bourquin measured[18]

$$\frac{\Gamma(\Omega^- \to \Xi^0\pi^-)}{\Gamma(\Omega^- \to \Xi^-\pi^0)} = 2.94 \pm 0.35$$

for the decuplet-octet transition. Because the Ω^- contains three strange quarks, the $\Delta I = 3/2$ amplitude is expected to be 20% of the $\Delta I = 1/2$ amplitude,[19] giving

$$\frac{\Gamma(\Omega^- \to \Xi^0\pi^-)}{\Gamma(\Omega^- \to \Xi^-\pi^0)} = 3 \pm 0.3$$

in agreement with experiment.

Improvements in experiment are necessary before a test of one of the protosuccesses of the standard model of the strong and electroweak

* This is no longer true. The Fermilab group (P. Cooper spokesman) reported new results on Σ^- (in Oct 84) which had

interactions can be made. This is the beginning of a dynamical understanding of the $\Delta I = 1/2$ rule in nonleptonic hyperon and kaon decays. The effective weak-interaction Hamiltonian for quarks is not that given by the GWS model alone. Finite, calculable (in principle) effects are induced by gluon exchanges. These come in two forms: initial- and final-state, etc., interactions as indicated in Fig. 6 and also "penguin" effects, such as shown in Fig. 7. The latter have no physical effects when the strong interactions are absent, as they can be absorbed into a weak-interaction wave-function renormalization of the quarks. Because of the vectorial coupling of the gluon, these penguin graphs induce effective nonleptonic right-handed charged-current interactions as well as effective strangeness-changing neutral-current interactions.

We say these calculations[17] are protosuccesses as they indicate enhancement of $\Delta I = 1/2$ processes. Unfortunately, these "short distance" calculations do not show sufficient relative (to $\Delta I = 3/2$) enhancement to explain the data. This alone may not be too unsatisfactory as there are additional "long distance" (current algebra) pieces that have not been included. However, there are reasons to question even the magnitude of the short distance enhancements.[20] Explicit one-loop calculations show that there may be significant omissions in the more popular "leading logarithm approximation" (or Operator Product Expansion) calculations.[21]

Nonetheless, this is an active area of theoretical effort.[22] If more detailed information on decay channels (final-state polarizations would be very important) could be obtained, many of the ambiguities might be resolved phenomenologically. Because they involve the dynamical interplay of the strong and weak interactions beyond the level of tree graphs, studies in this area offer deep tests of the full quantum field theory of the standard model.

C. Radiative Decays

The radiative decays $\Sigma^+ \to p\gamma$, $\Xi^0 \to \Sigma^0\gamma$, $\Xi^0 \to \Lambda\gamma$, $\Xi^- \to \Sigma^-\gamma$, and $\Omega^- \to \Xi^-\gamma$ are used to test QCD calculations (see Sec. II) and are sensitive to the contribution the penguin diagram makes to the process.

The decays fall into the general class of decay

$$B_1(P_1) \to B_2(P_2) + \gamma(k)$$

$$k = P_1 - P_2 \ ,$$

which are described by the transition matrix

$$M = \epsilon_\nu(k)\bar{U}(P_2)\left[a + b\gamma_5\right]\sigma_{\mu\nu}k_\mu U(P_1) \ .$$

ϵ_ν is the photon polarization, and a and b are the parity-conserving and parity-violating amplitudes, respectively. The amplitudes can be estimated by QCD calculations. They are related to the decay rate Γ and asymmetry parameter α by the equations

$$\Gamma = \frac{1}{\pi}\left(\frac{M_1^2 - M_2^2}{2M_1}\right)^3 (|a|^2 + |b|^2)$$

$$\alpha = \frac{2\mathrm{Re}(a^*b)}{|a|^2 + |b|^2} \ .$$

In the exact SU(3) limit assuming CP invariance, U-spin symmetry, and a current-current form of the weak interaction involving only left-handed currents, α is predicted to be zero.[23] Strong-interaction effects can be included via current algebra calculations and yield predictions typically about $\alpha = -0.25$ (Refs. 24, 25).

Other calculations to determine strong interaction effects employing dispersion relations to evaluate contributions of πN intermediate states have results ranging from -1.0 (Ref. 26) to $+0.8$ (Ref. 27) depending on input parameters. Theoretical reasons have been presented that rule against such large values of α from strong interactions and most predictions favor smaller values.[27,28]

Recently two papers have been independently published which predict a large asymmetry, $\alpha = -1$, as a result of a right-handed current between the charmed and strange quarks.[23,29] Such currents have been suggested to explain the nonleptonic $\Delta I = 1/2$ rule and the large ratio of nonleptonic to semileptonic weak decays.[30,31] Present high-energy neutrino data, most notably the $\langle y \rangle$ dependence of the reaction $\bar{\nu}N \to \mu^+ X$ and the large ratio $\sigma(\bar{\nu}N \to \mu^+ X)/\sigma(\nu N \to \mu^- X)$, are indicative of right-handed currents between the usual quarks and a heavier object.[32] Thus, there seems to be evidence

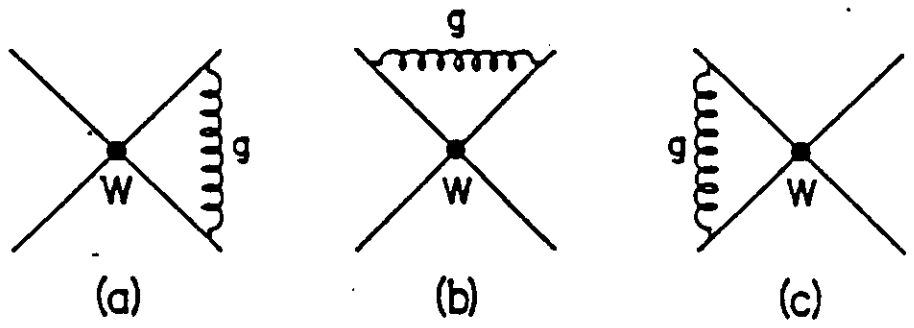

Fig. 6. Gluon exchange corrections for weak processes.

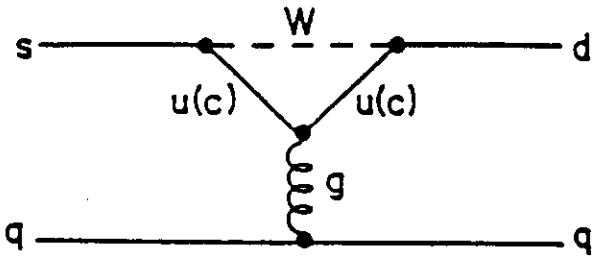

Fig. 7. Penguin diagram contribution to strangeness-changing processes.

for right-handed currents, and such currents can cause a large asymmetry in $\Sigma^+ \to p\gamma$.

The only measurement of α is the result of a bubble chamber experiment[33] and is

$$\alpha = -1.03^{+0.52}_{-0.42} .$$

This result is based on 61 events.

The value of α has taken on new significance as a result of the above ideas. The statistical quality and systematic uncertainties involved in the present measured value are quite poor. Because α is a fundamental and interesting parameter in the theory on the radiative decay of the Σ^+ hyperon, a new measurement with good statistics and the feature of small systematic error inherent in polarized target experiments is needed.

Within the framework of QCD the three types of quark diagrams shown in Fig. 8 are believed to contribute to the direct radiative decay. The four-quark diagram, not allowed for Ξ^- or Ω^- decays, is allowed for Ξ^0 decay. A comparison of Ξ^0 decay with Ξ^- and Ω^- decay then allows the four-quark diagram to be isolated. This type of analysis is being proposed by R. Poster at BNL using the Medium-Energy Separated Beam in conjunction with the Multiparticle Spectrometer.[34] Even assuming that the experiment of R. Poster is run, it is evident from Table III that LAMPF II can be used to make a substantial impact on the understanding of these decays.

D. Suppressed or Forbidden Decays

The increase of cleanly tagged hyperons anticipated at LAMPF II can be used to improve limits on a multitude of suppressed or forbidden decays. The following provides a list and discussion of a few possibilities together with current experimental limits.

1. Strangeness-Changing Neutral-Current Transitions. Strangeness-changing neutral-currents are suppressed by the GIM cancellation mechanism. Like kaon decays,[16] hyperon decays that involve such currents should exist in second-order in the electroweak interaction and be calculable in any renormalizable gauge theory.

A limit of

$$\frac{\Gamma(\Sigma^+ \to pe^+e^-)}{\Gamma(\Sigma^+ \to \text{all})} < 7 \times 10^{-6}$$

for such a process is given by Ang using a bubble chamber with a stopped-K^+ beam.[17]

2. $\Delta S = 2$ Transitions. No decay that violates the $|\Delta S|<1$ rule in first-order electroweak interaction is known to exist. Searches for such processes consequently are of fundamental importance.

The $\Delta S = 2$ transition $\Xi^0 \to p\pi^-$ was looked for by Gewenniger et al.[18] using the CERN neutral-hyperon beam. They set the limit

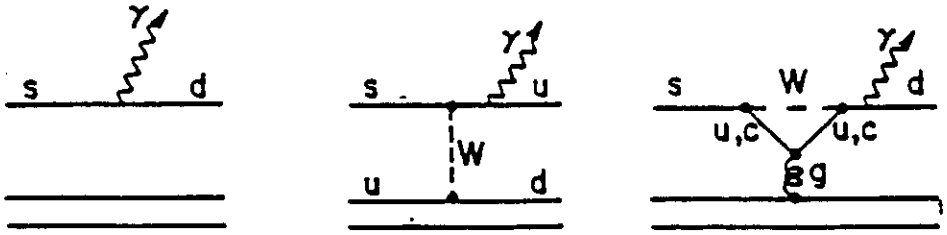

Fig. 8. Contributions to radiative hyperon decays.

TABLE III

RADIATIVE HYPERON DECAYS

Reaction	Author	Event	Branching Ratio[a]	α
$\Sigma^+ \to p\gamma$	Gershwin[13]	61	$(2.76 \pm 0.51) \times 10^{-3}$	$-1.03^{+0.52}_{-0.42}$
$\Xi^- \to \Sigma^-\gamma$	Yeh[15]	0/8150	$<1.1 \times 10^{-3}$	
$\Xi^0 \to \Lambda\gamma$	Yeh[15]	1	$(5 \pm 5) \times 10^{-3}$	
$\Xi^0 \to \Sigma^0\gamma$	Yeh[28]	0/507	$<6.5 \times 10^{-2}$	
$\Omega^- \to \Xi^-\gamma$	Bourquin[18]	0/2400	$<3.1 \times 10^{-3}$	

[a]Upper limits are at 90% confidence level as listed in Particle Group, Phys. Lett. 75B, 1 (1978).

$$\frac{\Gamma(\Xi^0 \to p\pi^-)}{\Gamma(\Xi^0 \to \Lambda\pi^0)} < 3.6 \times 10^{-5} .$$

Similarly, Bourquin in the CERN charged-hyperon beam set the limit[18]

$$\frac{\Gamma(\Omega^- \to \Lambda\pi^-)}{\Gamma(\Omega^- \to \text{all})} < 1.3 \times 10^{-3}$$

for Ω^- decay.

3. Flavor-Changing Neutral-Current Transitions. Flavor-changing neutral-current transitions are sensitive to new interactions that are expected from horizontal-symmetry models that relate generations.[16] Kane and Thun[19] comment that a search for such a process in Σ^+ decay may have advantages over such a search in kaon decay because the decay does not require a coupling to a pseudoscalar current, which would be sensitive to helicity suppression. However, the limit on the possible branding ratio for $\Sigma^+ \to p\mu e$ decay they set for such a process, based on the $K_L - K_S$ mass difference and the current $K_L \to \mu e$ branching ratio, is only $BR(\Sigma^+ \to p\mu e) \lesssim 10^{12}$. Obviously, to observe such a decay, clean and intense Σ^+ fluxes are needed as will be obtainable at LAMPF II.

REFERENCES

1. O. E. Overseth, High Energy Physics with Polarized Beams and Polarized Targets, Lausanne, 1980, C. Joseph and J. Soffer, Eds. (Birkhäuser Verlag, Basel, 1981), p. 114.

2. G. Bunce, High Energy Physics with Polarized Beams and Polarized Targets, Lausanne, 1980, C. Joseph and J. Soffer, Eds. (Birkhäuser Verlag, Basel, 1981), p. 141.

3. B. Anderssson, G. Gustafson, and G. Ingelman, Phys. Lett. 85B, 417 (1979).

4. T. DeGrand and R. L. Jaffe, Ann. Phys. 100, 425 (1976).

5. T. DeGrand, Ann. Phys., 101, 496 (1976).

6. R. Koniuk and N. Isgur, Phys. Rev. D21, 1868 (1980); K. T. Chad, N. Isgur and G. Karl, Phys. Rev. D23, 155 (1981).

7. D. Strottman, Phys. Rev. 18, 2716 (1978).

8. P. Dydak, F. L. Navarria, O. E. Overseth, P. Steffen, J. Steinberger, H. Wahl, et al., Nucl. Phys. B118, 1 (1977).

9. T. S. Mast, M. Alston-Garnjost, R. O. Bangerter, A. Barbero-Galtieri, L. K. Gershwin, F. T. Solmitz, and R. D. Tripp, Phys. Rev. Lett. 21, 1715 (1968).

10. J. Colas, C. Farwell, A. Ferrer, and J. Six, Nucl. Phys. B91, 253 (1975).

11. M. Kobayashi and T. Maskawa, Prog. Theor. Phys. 49, 652 (1973).

12. L. M. Chounet, J. M. Gaillard, and M. K. Gaillard, "Leptonic Decays of Hadrons," Phys. Rep. 4, 199 (1972).

13. A. Garcia and P. Kielanowski, Phys. Rev. D26, 1090 (1982).

14. Particle Data Group, Rev. Mod. Phys. 52, S12 (April 1980).

15. T. D. Lee et al., "Possible Detection of Parity Non-Conservation in Hyperon Decay," Phys. Rev. 30, 1367 (1957).

16. R. J. Hemingway, R. Armenteros, C. Dionisi, Ph. Gavillet, A. Gurtu, S. O. Holmgren, et al., "Ω⁻ Produced in K⁻p Reactions at 4.2 GeV/c," Nucl. Phys. B142, 205 (1978).

17. Finjord, "Ω⁻ Non-Leptonic Decays," Phys. Lett. 76B, 116 (1978).

18. M. Bourquin, R. M. Brown, Y. Chatelus, J. C. Chollet, A. Degré, D. Froidevaux, et al., "First Measurement of the Ω⁻ Decay Branching Ratios," Phys. Lett. 88B, 192 (1979).

19. O. E. Overseth, "Test of ΔI = 1/2 Rule for Hyperon Decays," Rev. Mod. Phys. 48, S242 (April 1976).

20. T. Goldman and D. Preston, Nucl. Phys. B217, 61 (1983).

21. M. K. Gaillard and B. W. Lee, Phys. Rev. D10, 897 (1974); G. Altarelli, R. K. Ellis, L. Maiani, and R. Petronzio, Nucl. Phys. B88, 215 (1975).

22. B. Desplanques, J. F. Donahue, and B. R. Holstein, Ann. Phys. 124, 449 (1980).

23. N. Vasanti, Phys. Rev. D13, 1889 (1976).

24. B. R. Holstein, Nuovo Cimento 2A, 561 (1971).

25. L. R. Ram Mohan, Phys. Rev. D3, 785 (1971).

26. I. Kimel, Lett. Nuovo Cimento 8, 166 (1973).

27. G. R. Farrar, Phys. Rev. D4, 212 (1971).

28. J. M. Reid, N. M. Trofimenkoff, Lett. Nuovo Cimento 9, 421 (1974); M. D. Scadron, L. R. Thebaud, Phys. Rev. D8, 2190 (1973).

29. M. A. Ahmed and G. G. Ross, Phys. Lett. 59B, 293 (1975).

30. F. A. Wilczek, A. Zee, R. L. Kingsley, and S. B. Treiman, Phys. Rev. D12, 2768 (1975).

31. A. De Rujula, H. Georgi, S. L. Glashow, Phys. Rev. Lett. 35, 69 (1975).

32. R. M. Barnett, "Restrictions on Models of the Weak Interactions," Phys. Rev. D15, 675 (1977).

33. L. K. Gershwin, M. Alston-Garnjost, R. O. Bangerter, A. Barbero-Galtieri, T. S. Mast, F. T. Solmitz, and R. D. Tripp, Phys. Rev. 188, 2077 (1969).

34. R. A. Poster et al., "AGS Proposal: Measurement of Hyperon Radiative Decay," E751 (1981).

35. N. Yeh, A. Caiglas, W. D. Smith, N. Zandl, C. B. Altay, A. Bridgewater, et al., Phys. Rev. D10, 3545 (1974).

36. T. W. L. Sanford, "Rare Kaon Decays at LAMPF II," Draft Proposal, LAMPF II (February 1982).

37. D. Ang, N. Ebenhöh, F. Eisele, R. Englemann, N. Filthuth, W. Fohlisch, et al., Z. Phys. 228, 151 (1969).

38. C. Geweniger, S. Gjesdal, G. Presser, P. Steffen, J. Steinberger, F. Vannucci, et al., Phys. Lett. B57, 193 (1975).

39. G. L. Kane and R. Thun, "Searches for Effects of Flavor-Changing Neutral Currents," Phys. Lett. 94B, 513 (1980).

Continuous Electron Beam Accelerator Facility

12000 Jefferson Avenue
Newport News, Virginia 23606
(804) 249-7100

Proposal Number: PR-89-024

Proposal Title: Radiative Decays of the Low-Lying Hyperons

Spokespersons/Contact Persons: G. Mutchler

Proposal Status at CEBAF:

The $\Lambda\gamma$ measurement may be carried out to the extent feasible in conjunction with the approved running of PR-89-004, the latter experiment being the primary determinant of running conditions. For the $\Sigma\gamma$ work deferral is recommended.

Dirk Walecka

John Dirk Walecka
Scientific Director

RICE

RICE UNIVERSITY

T. W. BONNER NUCLEAR LABORATORY
HOUSTON, TX 77251-1892

Tel. (713) 528-2159 FTS: 522-3141 & 3142 FAX: (713) 527-9033

E-Mail Nodes
BitNet: RICE
Arpanet: PHYSICS.RICE
Hepnet: FNAL::TAMHEP::RIPHYS::

October 31, 1989

Professor John Dirk Walecka
Scientific Director, CEBAF
12070 Jefferson Avenue
Newport News, Virginia 23606

Dear Professor Walecka:

Enclosed is our proposal "Radiative Decays of the Low Lying Hyperons," using the LAS. This proposal should be considered in conjunction with the proposal "Electromagnetic Production of Hyperons" R. Schumacher, Spokesman.

Sincerely,

G. S. Mutchler
Professor of Physics

CEBAF PROPOSAL COVER SHEET

This Proposal must be mailed to:

CEBAF
Scientific Director's Office
12000 Jefferson Avenue
Newport News, VA 23606

and received on or before OCTOBER 30, 1989

A. TITLE:

B. CONTACT PERSON:

ADDRESS, PHONE AND BITNET:

C. THIS PROPOSAL IS BASED ON A PREVIOUSLY SUBMITTED LETTER OF INTENT

☐ YES
☐ NO

IF YES, TITLE OF PREVIOUSLY SUBMITTED LETTER OF INTENT

D. ATTACH A SEPARATE PAGE LISTING ALL COLLABORATION MEMBERS AND THEIR INSTITUTIONS

==========

(CEBAF USE ONLY)

Letter Received_____

Log Number Assigned_____

By_____

CEBAF PROPOSAL COVER SHEET

This Proposal must be mailed to:

CEBAF
Scientific Director's Office
12000 Jefferson Avenue
Newport News, VA 23606

and received on or before OCTOBER 30, 1989

A. TITLE:

B. CONTACT PERSON:

ADDRESS, PHONE AND BITNET:

C. THIS PROPOSAL IS BASED ON A PREVIOUSLY SUBMITTED LETTER OF INTENT

☐ YES
☐ NO

IF YES, TITLE OF PREVIOUSLY SUBMITTED LETTER OF INTENT

D. ATTACH A SEPARATE PAGE LISTING ALL COLLABORATION MEMBERS AND THEIR INSTITUTIONS

==========

(CEBAF USE ONLY)

Letter Received_____

Log Number Assigned_____

By_____

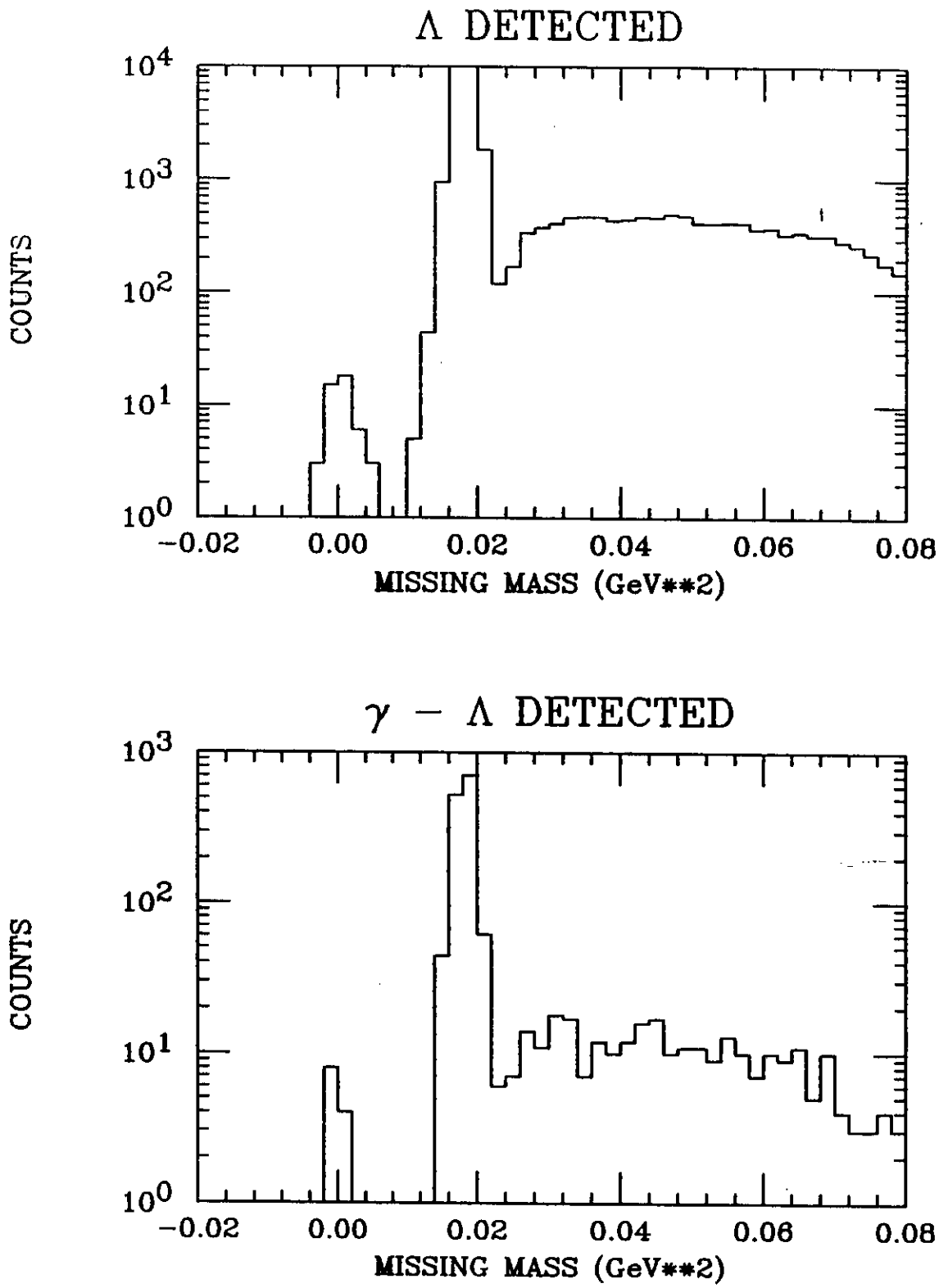

Figure 8: Missing mass spectrum of photon from reaction $\gamma p \rightarrow K^+ \Lambda(1405), \Sigma(1285) \rightarrow K^+ \gamma \Lambda$

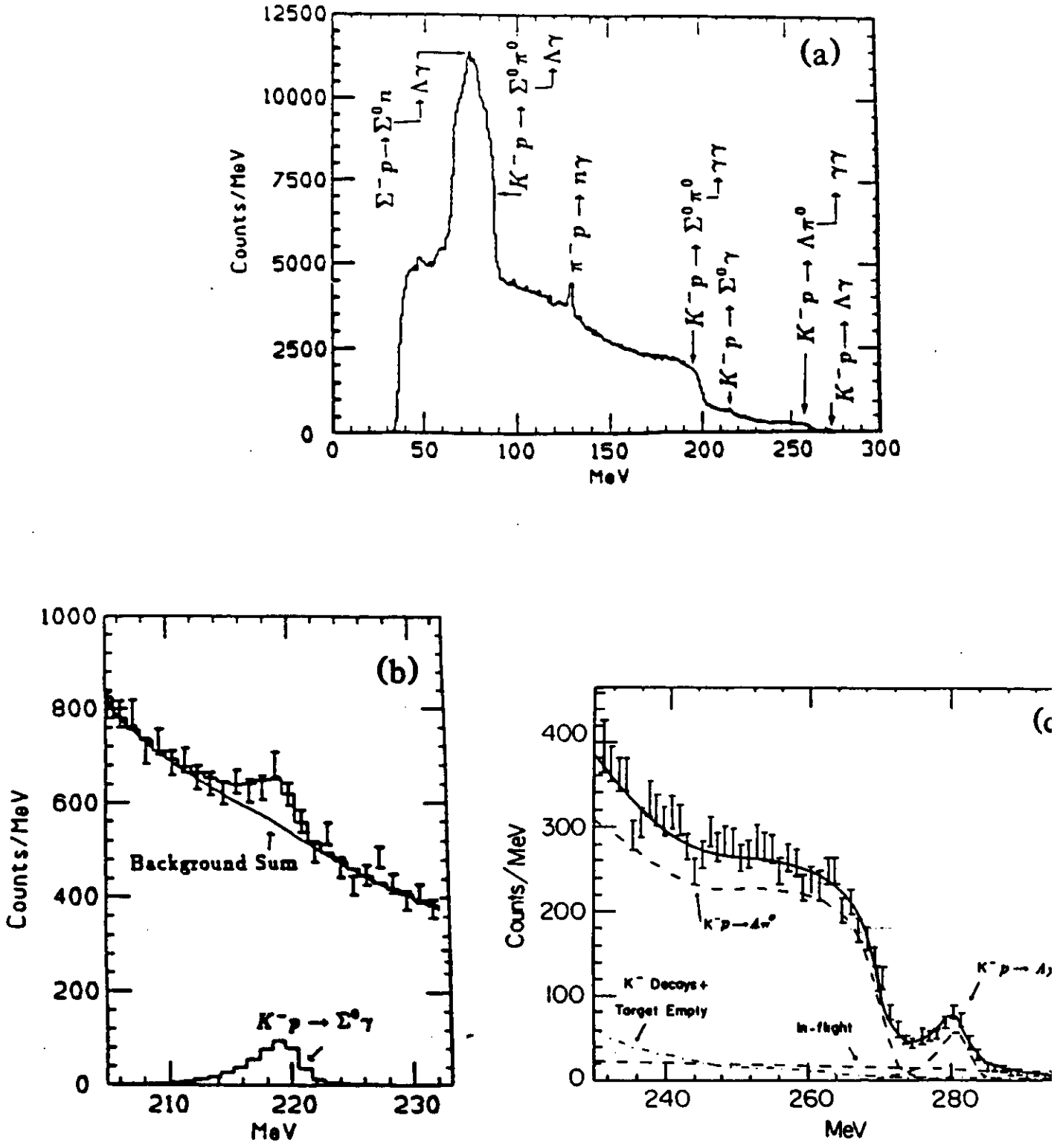

FIG. 2. (a) The experimental spectrum of data from one of the two running periods showing the two signal peaks plus backgrounds discussed in the text. (b) The region of the spectrum containing the $\Sigma^0\gamma$ signal. The smooth solid curve is the total background; the solid histogram is the fit to the data. The signal contribution to the fit is shown separately at the bottom of the figure. (c) The end-point region of the photon spectrum showing the $\Lambda\gamma$ radiative-capture peak and the end-point regi the π^0 decay photons from the $\Lambda\pi^0$ channel. The solid curve is the best fit. The background from K^- decays plus target em shown as a dot-dashed curve, while the contribution from in-flight interactions is shown by a dashed line. The latter are the inant contribution above the end point. The $\Lambda\gamma$ signal contribution is shown as a separate dashed line.

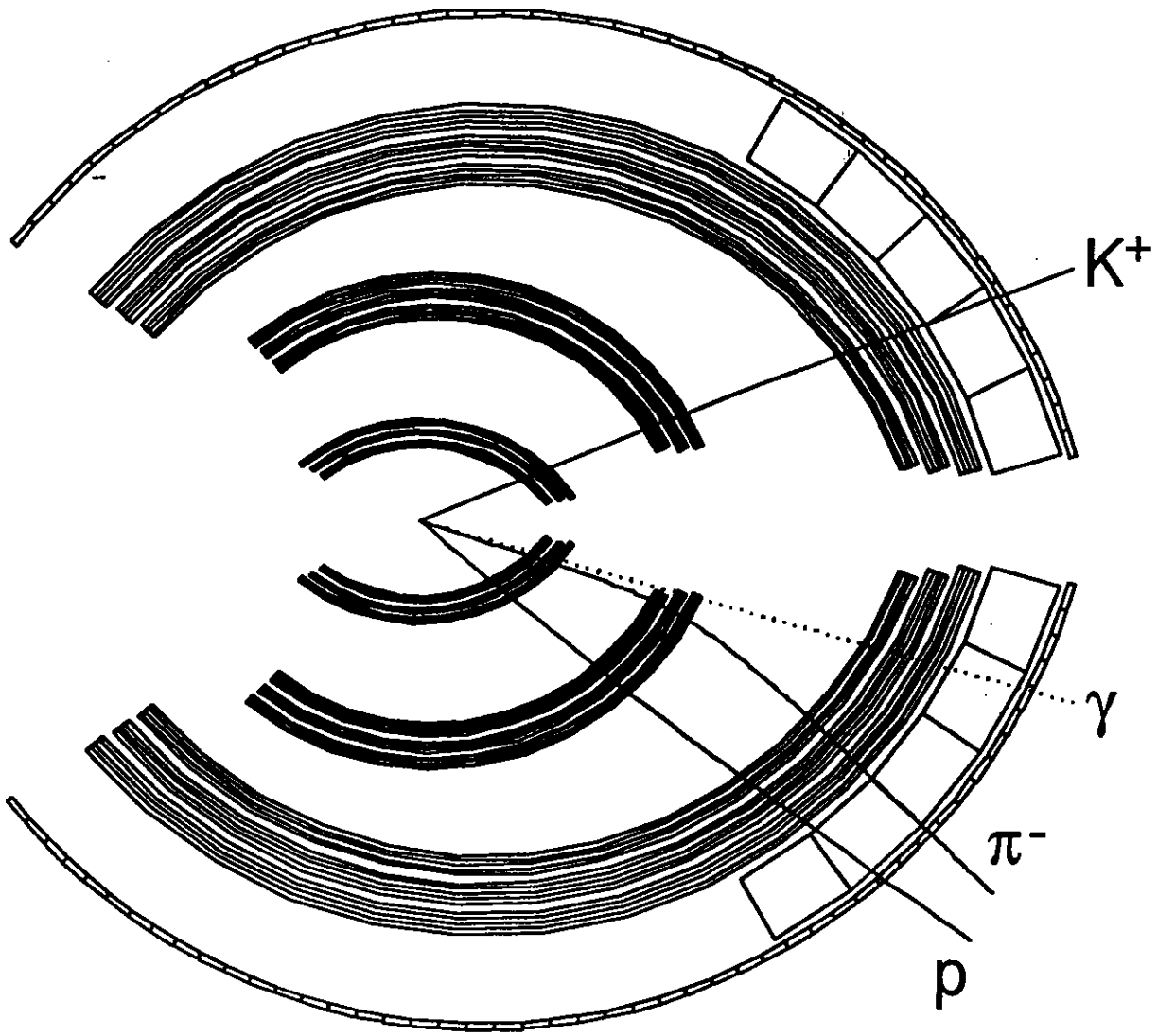

Figure 3: Typical $\gamma p \rightarrow K^+\Lambda^+ \rightarrow K^+ \gamma p\pi^-$ Event in LAS

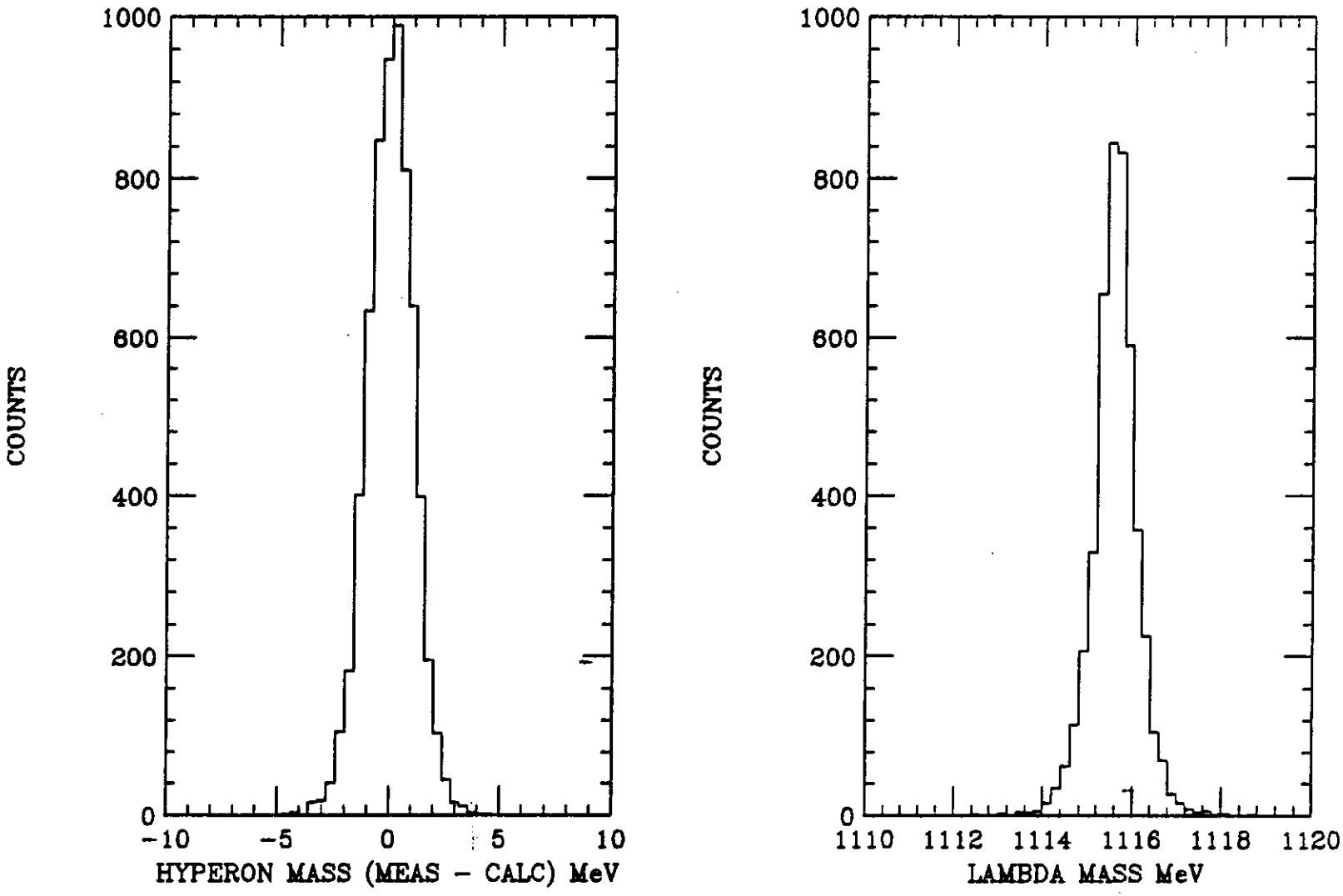

Figure 4: Mass resolution for $\gamma p \rightarrow K^{+}\Lambda(1520)$

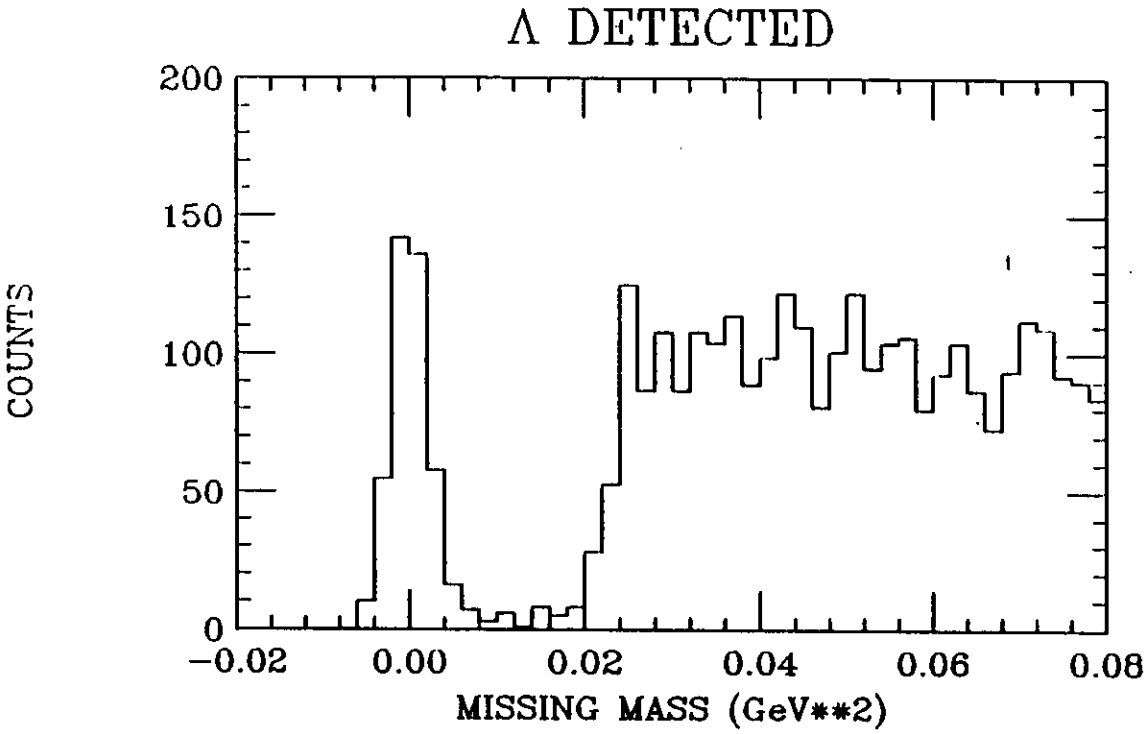

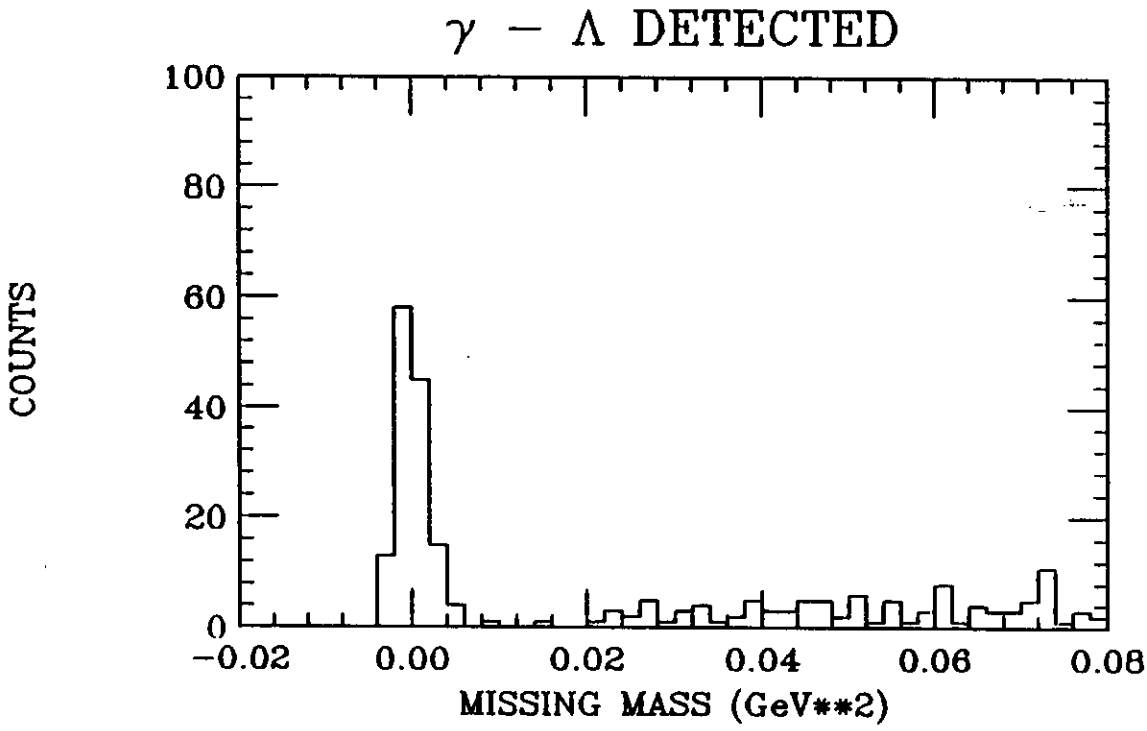

Figure 5: Missing mass spectrum of photon from reaction $\gamma p \to K^+ \Lambda(1520) \to K^+ \gamma \Lambda$

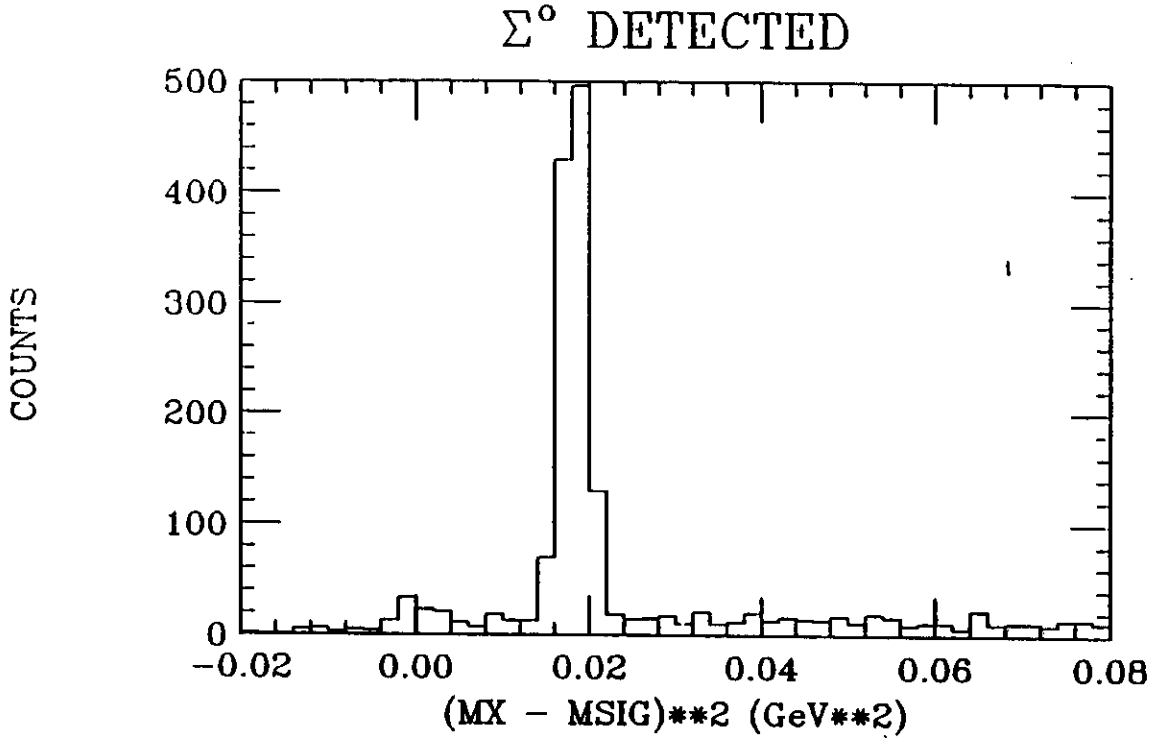

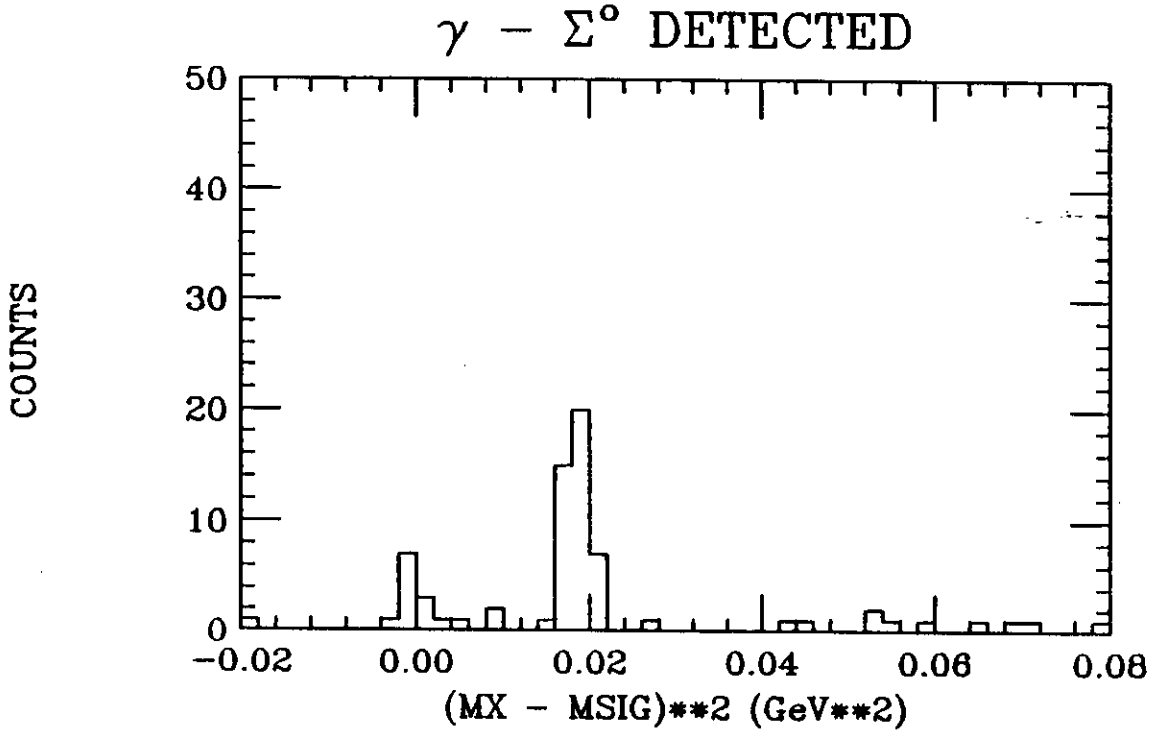

Figure 6: Missing mass spectrum of photon from reaction $\gamma p \rightarrow K^{+} \Lambda(1520) \rightarrow K^{+} \gamma \Sigma^{0}$

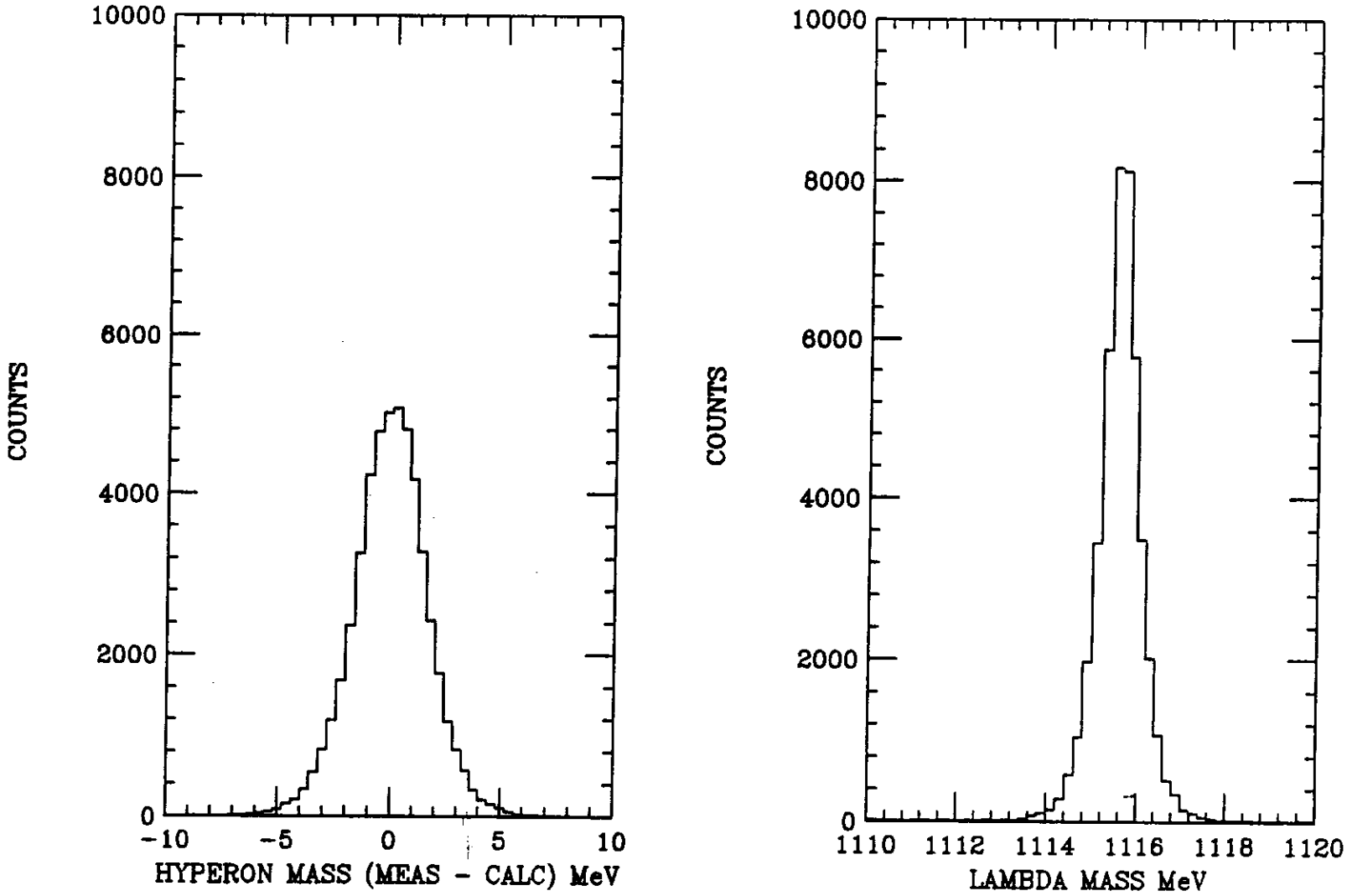

Figure 7: Mass resolution for $\gamma p \rightarrow K^{+}\Lambda(1405)$ and $\gamma p \rightarrow K^{+}\Sigma(1385)$